

# TTL Proteins Scaffold Brassinosteroid Signaling Components at the Plasma Membrane to Optimize Signal Transduction in Arabidopsis

Vítor Amorim-Silva<sup>1</sup>, Álvaro García-Moreno<sup>1</sup>, Araceli G. Castillo<sup>2</sup>, Naoufal Lakhssassi<sup>3</sup>, Alicia Esteban del Valle<sup>1</sup>, Jessica Pérez-Sancho<sup>1</sup>, Yansha Li<sup>4</sup>, David Posé<sup>1</sup>, Josefa Pérez-Rodríguez<sup>1</sup>, Jinxing Lin<sup>5</sup>, Victoriano Valpuesta<sup>1</sup>, Omar Borsani<sup>6</sup>, Cyril Zipfel<sup>7,8</sup>, Alberto P. Macho<sup>4,7</sup>, Miguel A. Botella<sup>1,9,\*</sup>

<sup>1</sup>Departamento de Biología Molecular y Bioquímica. Instituto de Hortofruticultura Subtropical y Mediterránea “La Mayora”, Universidad de Málaga-Consejo Superior de Investigaciones Científicas (IHSM-UMA-CSIC), Universidad de Málaga, Campus Teatinos, 29071 Málaga, Spain

<sup>2</sup>Departamento de Biología Celular, Genética y Fisiología. Instituto de Hortofruticultura Subtropical y Mediterránea “La Mayora”, Universidad de Málaga-Consejo Superior de Investigaciones Científicas (IHSM-UMA-CSIC), Universidad de Málaga, Campus Teatinos, 29071 Málaga, Spain

<sup>3</sup>Department of Plant, Soil and Agricultural Systems, Southern Illinois University, Carbondale, IL 62901, USA.

<sup>4</sup>Shanghai Center for Plant Stress Biology, CAS Center for Excellence in Molecular Plant Sciences, Shanghai Institutes of Biological Sciences, Chinese Academy of Sciences (CAS), Shanghai, China

<sup>5</sup>College of Biological Sciences and Technology, Beijing Forestry University, Beijing 100083, China

<sup>6</sup>Departamento de Biología Vegetal, Laboratorio de Bioquímica, Facultad de Agronomía Universidad de la República, Montevideo, Uruguay

<sup>7</sup>The Sainsbury Laboratory, University of East Anglia, Norwich Research Park, Norwich, NR4 7UH, United Kingdom.

<sup>8</sup>Institute of Plant and Microbial Biology and Zurich-Basel Plant Science Center, University of Zurich, CH-8008 Zurich, Switzerland.

<sup>9</sup>Lead Contact

\*Correspondence: [mabotella@uma.es](mailto:mabotella@uma.es)

**Short title:** TTL proteins function in BR signaling

**One-sentence summary:** Plant-specific TTL proteins function as positive regulators of BR responses likely by bringing together signaling components at the plasma membrane.

The author responsible for distribution of materials integral to the findings presented in this article in accordance with the policy described in the Instructions for Authors ([www.plantcell.org](http://www.plantcell.org)) is: Miguel A. Botella ([mabotella@uma.es](mailto:mabotella@uma.es)).

## Abstract

Brassinosteroids (BRs) form a group of steroidal hormones essential for plant growth, development and stress responses. BRs are perceived extracellularly by plasma membrane receptor-like kinases, which activate an interconnected signal transduction cascade, leading to the transcriptional regulation of BR-responsive genes. *TETRATRICOPEPTIDE THIOREDOXIN-LIKE (TTL)* genes are specific for land plants and their encoded proteins are defined by the presence of protein-protein interaction motives, i.e. an intrinsic disordered region at the N-terminus, six tetratricopeptide repeat domains and a C-terminus with homology to thioredoxins. TTL proteins thus likely mediate the assembly of multiprotein complexes. Phenotypic, molecular and genetic analyses show that TTL proteins are positive regulators of BR signaling in *Arabidopsis thaliana*. TTL3 directly interacts with a constitutively active BRASSINOSTEROID INSENSITIVE1 (BRI1) receptor kinase, BRI1-SUPPRESSOR1 (BSU1) phosphatase and the BRASSINAZOLE RESISTANT1 (BZR1) transcription factor and associates with BR-SIGNALING KINASE1 (BSK1), BRASSINOSTEROID INSENSITIVE2 (BIN2) kinases but not with BRI1-ASSOCIATED KINASE 1 (BAK1). A functional TTL3-GFP shows dual cytoplasmic-plasma membrane localization. Depleting the endogenous BR content reduces plasma membrane localization of TTL3-GFP, while increasing BR content causes its plasma membrane relocalization, where it strengthens the association of BR signaling components. Our results reveal that TTL proteins promote BR responses and suggest that TTL proteins may function as scaffold proteins by bringing together cytoplasmic and plasma membrane BR signaling components.

## Introduction

Brassinosteroids (BRs) are a family of growth-promoting hormones with essential roles in a wide range of developmental and physiological processes (Jaillais and Vert, 2016; Chaiwanon et al., 2016; Belkhadir and Jaillais, 2015). However, in addition to their well-established function in growth, essential roles in the trade-off between growth and tolerance to biotic and abiotic stress episodes are now being unveiled (Lozano-Durán and Zipfel, 2015; Nolan et al., 2017; Zhang et al., 2016; Tian et al., 2018). BRs are perceived at the plasma membrane by ligand-induced heterodimers of the receptor kinases BRASSINOSTEROID INSENSITIVE1 (BRI1) and SOMATIC EMBRYOGENESIS RECEPTOR KINASE (SERK) protein family members, which activates an interconnected signal transduction cascade, leading to the transcriptional regulation of BR-responsive genes (Belkhadir and Jaillais, 2015). BRI1 KINASE INHIBITOR 1 (BKI1) dissociates from activated BRI1, which phosphorylates the BSK family proteins BR-SIGNALING KINASE1 and 3 (BSK1 and BSK3) and the CONSTITUTIVE DIFFERENTIAL GROWTH1 (CDG1), which in turn activate the BRI1-SUPPRESSOR1 (BSU1) phosphatase (Belkhadir and Jaillais, 2015; Wang et al., 2014; Ren et al., 2019). Then, the active (phosphorylated) BSU1 leads to dephosphorylation and inactivation of the glycogen synthase kinase 3 (GSK3)-like BRASSINOSTEROID INSENSITIVE2 (BIN2). In the absence of BRs, BIN2 is active and phosphorylates the two homologous transcription factors BRASSINAZOLE RESISTANT1 (BZR1) and BRI1-ETHYL METHANESULFONATE SUPPRESSOR 1 (BES1/BZR2), which results in their inactivation and degradation (Belkhadir and Jaillais, 2015; Wang et al., 2014). By contrast, when BR is present, BIN2 is inactivated and degraded by the proteasome mediated by the F-box E3 ubiquitin ligase KINK SUPPRESSED 1 in *bzr1-1D* (KIB1) (Zhu et al., 2017), which leads to both the stabilization and activation of BZR1 and BES1, and therefore to transcriptional regulation of BR-responsive genes (Belkhadir and Jaillais, 2015; Wang et al., 2014).

In Arabidopsis, the *TETRATRICOPEPTIDE THIOREDOXIN-LIKE (TTL)* gene family is composed of four members (*TTL1* to *TTL4*) and mutations in *TTL1*, *TTL3*, and *TTL4* cause reduced growth under abiotic stresses such as salinity and drought (Rosado et al., 2006; Lakhssassi et al., 2012; Ceserani et al., 2009). This stress hypersensitivity is exacerbated in double and triple *tll* mutants (Lakhssassi et al., 2012). *TTL2* is specifically expressed in pollen grains and does not have a role in stress tolerance, but it is important for male sporogenesis (Lakhssassi et al., 2012). *TTL* genes encode proteins with a common modular architecture containing six Tetratricopeptide Repeat (TPR) domains distributed in specific positions throughout the sequence and a C-terminal sequence with homology to thioredoxins (Rosado et al., 2006; Lakhssassi et al., 2012). TPR domains are well-described protein-protein interaction modules; however, how *TTL* proteins function mechanistically in stress tolerance remains elusive.

Several lines of circumstantial evidence point to a role of TTL proteins in BR responses, which open the possibility of a direct link between stress tolerance and BR-signaling by the TTL proteins. First, the TTL3 protein, whose gene is the most highly expressed among the *TTL* gene family, was identified as an interacting partner of the activated (phosphorylated) cytoplasmic domain of VASCULAR HIGHWAY1/BRI1-LIKE RECEPTOR KINASE2 (BRL2). BRL2 has a role in vascular development and belong to the BRI family (Ceserani et al., 2009), although BRL2 cannot bind BRs (Belkhadir, 2015). Second, a *ttl3* mutant showed altered growth in the presence of exogenous BRs (Ceserani et al., 2009). Third, TTL proteins are predicted to interact and function as co-chaperones of Hsp90 (Prasad et al., 2010), which has been recently identified to have important roles in BR signaling by interacting with specific BR signaling components (Samakovli et al., 2014; Shigeta et al., 2015; 2014; Lachowiec et al., 2013). Fourth, a triple Arabidopsis lines with T-DNA insertions in *TTL1*, *TTL3*, and *TTL4* shows defects in vasculature development and male sporogenesis, hallmarks of BR defective mutants (Yang et al., 2011; Lakhssassi et al., 2012). Finally, *TTL1*, *TTL3*, and *TTL4* are specifically induced by BR application but not by other hormones (Prasad et al., 2010).

Based on phenotypic, molecular, and genetic analyses, we show that *TTL1*, *TTL3*, and *TTL4* genes, in addition to their reported role in abiotic stress tolerance, are positive regulators of BR signaling. The well-described TPR protein interaction modules of TTL proteins and their role in the assembly of multiprotein complexes (Blatch and Lässle, 1999; D'Andrea and Regan, 2003; Yang et al., 2005) led us to hypothesize that these proteins could function as a scaffold for BR signaling. Indeed, we show that TTL3 interacts with constitutively active BRI1, BSU1 and BZR1 and associates *in vivo* with most BR signaling components with the exception of BAK1. We also show that a functional TTL3 tagged with a Green Fluorescent Protein (GFP) shows a dual cytoplasmic and plasma membrane localization that is dependent on endogenous BR content. Furthermore, TTL3 greatly enhances the interaction between BSK1 and BZR1 at the plasma membrane and suppresses the BIN2-promoted cytoplasmic retention of BZR1-GFP. Together, we reveal that TTL proteins function as positive regulators of BR signaling likely by bringing together signaling components at the plasma membrane.

## Results

### Interaction analysis of TTL3 with BRI1

The TTL3 protein, also known as VH1- interacting tetratricopeptide repeat (TPR)-containing protein (VIT1), has been identified as an interactor of the activated (phosphorylated) cytoplasmic

domain of BRL2 (Ceserani et al., 2009), a receptor kinase of the BRI1 family with a role in vascular development (Caño-Delgado et al., 2004; Ceserani et al., 2009). *TTL3* belongs to a family of 4 genes (*TTL1* to *TTL4*) in *Arabidopsis* (Rosado et al., 2006; Lakhssassi et al., 2012). While *TTL1*, *TTL3*, and *TTL4* show ubiquitous expression, *TTL2* expression is restricted to pollen grains. We confirmed the reported defects in vein formation using a different *ttl3* mutant allele (Supplemental Figure 1A), and showed that mutations in *TTL1* and *TTL4*, but not *TTL2*, also caused venation defects that were markedly enhanced in a triple *ttl1 ttl3 tt4* mutant (from now on referred to as *ttl134*) (Supplemental Figure 1A).

TTL3 has been proposed to be an adaptor protein of BRL2 that, through association with other proteins modulate vein formation (Ceserani et al., 2009). TTL3, as other TTL proteins from other plant species (Rosado et al., 2006; Lakhssassi et al., 2012), are characterized by the presence of 6 tetratricopeptide repeats (TPR) and a C-terminal domain with homology to thioredoxins. An *in silico* structural analysis of TTL3 predicts the presence of an intrinsically disordered region (IDR) at the N-terminus (Supplemental Figure 2) with the rest of the protein forming a horseshoe-shaped structure composed of multiple helix-turn-helix motifs (Figure 1A). This structure is consistent with TTL3 being involved in protein-protein interactions and the assembly of multi-protein complexes (Blatch and Lässle, 1999; D'Andrea and Regan, 2003; Yang et al., 2005).

The similarity between BRL2 and BRI1 kinase domains (Supplemental Figure 3) suggested that TTL3 could also interact with the BRI1 cytoplasmic domain. We therefore tested the direct interaction of TTL3 with the BRI1 cytoplasmic region, which includes the juxta-membrane (JM), the kinase domain and carboxy-terminal (CT) domain (BRI1<sub>cyt</sub>) (Figure 1B). While BRI1<sub>cyt</sub> was soluble when fused to an MBP tag (Supplemental Figure S4), we were unable to produce full-length TTL3 protein fused to GST despite many attempts. This low stability was probably caused by the presence of the IDR (Habchi et al., 2014). Accordingly, we produced in *E. coli* two different fragments: TTL3 lacking the N-terminus IDR (TTL3 $\Delta$ N1) and TTL3 containing the TRLX domain (TTL3 $\Delta$ N3) (Figure 1C and Supplemental Figure 4). Using an *in vitro* GST pull-down assay, we did not detect an interaction between BRI1<sub>cyt</sub> and either TTL3 $\Delta$ N1 or TTL3 $\Delta$ N3 (Figure 1C and 1D). Because the activation of BRI1 is dependent on BRI1-ASSOCIATED KINASE 1 (BAK1) transphosphorylation on specific residues at the JM and CT (Wang et al., 2008), we next used a BAK1-independent BRI1 constitutively active (phosphomimetic) form BRI1<sub>cyt</sub><sup>JMCT9D</sup>. In this mutant version, nine serines and threonines have been substituted by aspartic acid at the JM and CR domains (Wang et al., 2008) (Figure 1B). In this case, BRI1<sub>cyt</sub><sup>JMCT9D</sup> was pulled down by TTL3 $\Delta$ N1, but not by TTL3 $\Delta$ N3 (Figure 1C and 1D). This indicates that TTL3 predominantly interacts with active BRI1, and that this interaction occurs through the TPR domains, but not the TRLX domain of TTL3.

Next, we investigated this interaction *in vivo* by performing co-immunoprecipitation (Co-IP) assays after transient expression of tagged full-length TTL3 and BRI1 in *Nicotiana benthamiana*. After immunoprecipitation of GFP-TTL3 and free GFP using GFP-Trap beads, we detected a strong specific interaction between GFP-TTL3 and BRI1-HA (Figure 1E). Additional Co-IP experiments using a C-terminal GFP-tagged TTL3 protein (TTL3-GFP) co-expressed with BRI1-HA (Supplemental Figure 5A) and BRI1-GFP co-expressed with TTL3-HA (Supplemental Figure 5B) further confirmed the TTL3-BRI1 interaction and indicated that the position and tag used in the Co-IP experiments does not affect their *in planta* interaction.

We further used Co-IP assays to map the TTL3 domains required for the interaction with BRI1. We performed this analysis *in planta* to determine the possible role of the IDR domain in the interaction, which was not possible using *in vitro* assays. We generated a series of truncated TTL3 fragments with deletions at the N-terminus (TTL3 $\Delta$ N1, TTL3 $\Delta$ N2, TTL3 $\Delta$ N3) and at the C-terminus (TTL3 $\Delta$ C1, TTL3 $\Delta$ C2) (Figure 1C), transcriptionally fused these fragments to GFP at the N-terminus, and co-expressed these constructs with BRI1-HA in *N. benthamiana* leaves. All expressed proteins showed the expected molecular size (Figure 1E, Input). TTL3 $\Delta$ C1 and TTL3 $\Delta$ C2 truncated proteins, both lacking the TRLX domain, showed lower accumulation than the others (Figure 1E, Input), suggesting that TRLX is important for protein stabilization.

The full-length TTL3 and three out of the five truncated TTL3 proteins, *i.e.* GFP-TTL3 $\Delta$ N1, GFP-TTL3 $\Delta$ N2, and GFP-TTL3 $\Delta$ C2, which all having in common TPR3 to TPR6 (Figure 1C), co-immunoprecipitated BRI1-HA with different efficiency, indicating that these domains are essential for the interaction, which is consistent with the *in vitro* data (Figure 1D). To quantify the interaction of the different TTL protein fragments and BRI1, the amount of co-immunoprecipitated BRI1-HA was normalized relative to the amount of protein input (Figure 1E). The strongest interaction occurs with the full-length TTL3 protein, indicating that all domains contribute to stabilize the interaction with BRI1. A lower but similar interaction was observed with GFP-TTL3 $\Delta$ N1 and GFP-TTL3 $\Delta$ N2, both containing the TRLX domain, indicating that this domain is important for stabilizing the interaction but is not sufficient for the *in vitro* or *in vivo* interaction with BRI1 (Figure 1C and 1E). Consistent with this, removing the TRLX region in GFP-TTL3 $\Delta$ C2 greatly reduced the interaction between TTL3 and BRI1 (Figure 1C-1E).

Finally, the interaction between BRI1 and TTL3 was also investigated using bimolecular fluorescence complementation (BiFC) assays in *N. benthamiana* leaves, which provide additional information about the subcellular localization of the interaction. Co-expression of TTL3-nYFP with BRI1-cYFP or BRI1-nYFP with TTL3-cYFP (Supplemental Figure 6) reconstituted functional YFP proteins at the plasma membrane, confirming the interaction and consistent with the plasma membrane localization of BRI1.

BAK1, also known as SOMATIC EMBRYOGENESIS RECEPTOR KINASE3 (SERK3), and other SERK proteins are transmembrane kinases that function as BR co-receptors (Ma et al., 2016). Similar Co-IP experiments using TTL3-GFP and BAK1 transiently co-expressed in *N. benthamiana* indicated that, contrary to BRI1, TTL3 does not associate *in vivo* with BAK1 (Supplemental Figure 5C). This result was verified by BiFC assays in *N. benthamiana* leaves since confocal microscopy analyses revealed that co-expression of TTL3-nYFP with BAK1-cYFP (Supplemental Figure 6A) and also BAK1-nYFP with TTL3-cYFP (Supplemental Figure 6B) did not reconstitute functional YFP proteins. To confirm that BiFC BAK1 constructs were functional, we performed a BiFC between BRI1 and BAK1 and observed weak but positive signals (Supplemental Figure 6A and 6B)

### **TTL proteins play a positive role in BR signaling**

The interaction of TTL3 with BRI1 supports a role for TTL3 in BR signaling. Furthermore, previous expression analyses indicate that *TTL1*, *TTL3*, and *TTL4* transcripts are induced by BR (Prasad et al., 2010), which is also supported by available public transcriptomic data (Supplemental Figure 7A). This up-regulation of the *TTL* genes in response to BR was confirmed at the cellular level by analyzing transgenic plants transformed with the reporter  $\beta$ -glucuronidase gene driven by each of the *TTL* promoters (Supplemental Figure 7B).

We next analyzed the sensitivity to epibrassinolide (eBL) by measuring root growth in the presence or absence of exogenous 100 nM eBL in wild type Col-0, single *tfl* mutants, the triple *tfl134* mutant and *bak1-4*, a well-established mutant affected in BR responses (Gou et al., 2012; He et al., 2007; Chinchilla et al., 2007; Schwessinger et al., 2011). Single *tfl* mutants, the *tfl134* mutant, and the *bak1-4* mutant showed a similar root growth to Col-0 in control conditions (Figure 2A and Supplemental Figure 8A). However, *bak1-4*, *tfl1*, *tfl3*, and *tfl4* show increased root length compared to the Col-0 control or *tfl2* in the presence of eBL (Figure 2A and Supplemental Figure 8B). The lack of *tfl2* sensitivity to BR is consistent with the pollen-specific expression of *TTL2* (Lakhssassi et al., 2012). This decreased sensitivity to eBL of single *tfl* mutants was strongly enhanced in *tfl134* (Figure 2A and Supplemental Figure 8B). Root growth sensitivity to eBL of the *tfl134* mutant was then compared, in addition to *bak1-4*, to well characterized genotypes affected in BR responses such as *serk1-1* and the double *serk1-1 bak1-4* mutant (Gou et al., 2012). In control conditions, all genotypes grew similar to Col-0, with the exception of *serk1-1 bak1-4*, which showed reduced root growth (Figure 2B and Supplemental Figure 8C) as previously reported (van Esse et al., 2013; Du et al., 2012). In the presence of 100 nM eBL, the root growth reduction of the Col-0 control was significantly higher than for the rest of the genotypes, including *tfl134* (Figure 2B and Supplemental Figure 8D), while the *serk1-1 bak1-4* double mutant was almost completely insensitive to eBL, as it showed a similar root growth in control and eBL-supplemented media.

Hypocotyl elongation in the dark is dependent on active BR signaling (Bernardo-García et al., 2014) and therefore it was analyzed in *tll3*, *tll134* and *bak1-4* as a read-out of defective BR signaling (Zhang et al., 2015). As previously reported, *bak1-4* showed a reduction in hypocotyl elongation relative to Col-0 (Li et al., 2002; Nam and Li, 2002) (Figure 2C and Supplemental Figure 8E). Similar to *bak1-4*, *tll3* and *tll134* mutants presented shorter hypocotyls than Col-0 (Figure 2C and Supplemental Figure 8E).

To investigate the contribution of *TTL* genes to BR responses at the molecular level, we first studied the expression of the BR-regulated genes *CPD1* and *DWF4* in Col-0, *bak1-4*, and the triple *tll134* mutants. As shown in Figure 2D, *DWF4* and *CDP1* expression was around two-fold higher in *tll134* and *bak1-4* compared to the Col-0 control. This increased *CPD1* and *DWF4* expression has been reported for BR signaling mutants such as *bri1-5* (Wang et al., 2016), *bri1-301* (Gou et al., 2012) and *bik1* (Lin et al., 2013), and is caused by a lack of feedback regulation in the expression of these biosynthetic genes (Tanaka et al., 2005; Vriet et al., 2013; Chung and Choe, 2013). Second, we investigated the phosphorylation status of BES1 in Col-0 and the *tll134* mutant in response to eBL. Because the BR biosynthetic genes *DWF4* and *CDP1* are already induced in *tll134*, to fully capture the BR signaling capacity of *tll134*, we pretreated the seedlings with the BR biosynthesis inhibitor brassinazole (BRZ). Without BR treatment, a strong signal of phosphorylated BES1 (pBES1) and a weak signal of unphosphorylated (BES1) are present in Col-0 and *tll134* (Figure 2E). While 10 nM eBL caused an increase of dephosphorylated BES1 in Col-0 after 30 and 60 min, eBL caused little dephosphorylation of pBES1 in *tll134* seedlings (Figure 2E), confirming a defective BR signaling in *tll134*.

Despite the role exerted by *TTL* genes in BR responses, *tll134* adult plants do not exhibit obvious growth defects when under short-day or long-day photoperiod (Figure 3A and Supplemental Figure 9A). Phenotypic defects in BR sensitivity are often revealed in adult plants when mutations in potential BR signaling components are combined with weak *bri1* alleles (Schwessinger et al., 2011; Kim and Wang, 2010; Nam and Li, 2002). Therefore, we generated and analyzed the phenotype of a quadruple homozygous *tll134 bri1-301* mutant. When grown in short-days, the *bri1-301* mutant displays a semi-dwarf cabbage-like rosette, a phenotype that was enhanced in the *tll134 bri1-301* quadruple mutant (Figure 3A). *tll134 bri1-301* plants have fewer leaves than *bri1-301* plants (Supplemental Figure 9B), and the younger leaves were considerably smaller in *tll134 bri1-301* than in *bri1-301* plants of the same age (Figure 3B). A stronger dwarf phenotype in *tll134 bri1-301* relative to the weak *bri1-301* mutant was also observed in long-day grown plants (Supplemental Figure 9A). *tll134 bri1-301* also shows enhanced defects in seedling root growth (Figure 3C and Supplemental Figure 9C) and hypocotyl elongation (Figure 3D) relative to *bri1-301*. Next, we determined the root growth BR sensitivity of *tll134 bri1-301* relative to Col-0, *tll134* and

*bri1-301* (Ren et al., 2019). The *ttl134 bri1-301* seedlings exhibited less root growth inhibition than *bri1-301* seedlings when grown on 500 nM of BL (Figure 3E).

The gain-of-function *bes1-D* mutant shows constitutive BR responses, including higher elongation of hypocotyl and petioles due to increased levels of BES1 protein (Yin et al., 2002) (Figure 3A and 3D). A *ttl134 bes-1D* quadruple mutant displays shorter hypocotyls and petioles than *bes1-D*, (Figure 3A, 3D and Supplemental Figure 9D). This indicates that mutations in *TTL* genes reduce BR responses of *bes1-D*. Together, these results indicate that the TTLs play a positive role in the regulation of BR responses.

### **BRs regulate the cytoplasmic/plasma membrane localization of TTL3**

To further explore how TTL3 functions in BR signaling, we analyzed its subcellular localization. Although the BiFC interaction of TTL3 with BRI1 suggests a plasma membrane localization of TTL3, expression of a C-terminal GFP-tagged TTL3 in *N. benthamiana* indicated a predominant cytoplasmic localization in basal conditions (Supplemental Figure 10A). However, plasmolyzed cells show the presence of GFP-TTL3 in Hechtian strands, indicating that TTL3 also associated with the plasma membrane (Supplemental Figure 10B). To gain further insight into TTL3 localization, a genomic fragment including a 1.7-kb *TTL3* promoter region upstream of the start codon was transcriptionally fused to GFP to generate the *TTL3p:TTL3g-GFP* construct and transformed into both *ttl3* and *ttl134* mutants using *A. tumefaciens*. After confocal analysis of a large number of independent stable transgenic lines, we selected two homozygous lines, one in the *ttl3* background (hereafter referred to as *TTL3-GFP 1.2*) and the other in the *ttl134* background (*TTL3-GFP 2.4*), which presented noticeable fluorescence signals. Venation defects of *ttl3* and *ttl134* were restored to levels similar to Col-0 in *TTL3-GFP 1.2* and *TTL3-GFP 2.4*, (Supplemental Figure 1B). Furthermore, root growth of *TTL3-GFP 1.2* (Supplemental Figure 11A and 11B) and *TTL3-GFP 2.4* (Figure 4A-4C) were restored to wild type levels in the presence of eBL, indicative of a functional TTL3-GFP protein.

We then used *TTL3-GFP 2.4* (which showed a stronger fluorescence signal than *1.2*) to analyze the cellular and subcellular localization of TTL3. Examination under a stereomicroscope indicated that TTL3-GFP accumulated mainly at the root tip and the hypocotyl of Arabidopsis seedlings (Figure 4D). This accumulation coincides with cells that undergo strong BR signaling leading to active growth, and highly resembles the accumulation pattern of BRI1-GFP (Wilma van Esse et al., 2011; Fàbregas et al., 2013; Geldner et al., 2007). Cellular analysis using confocal microscopy was performed in 3-day-old roots, simultaneously localizing TTL3-GFP with the FM4-64, a lipophilic red dye that labels the plasma membrane and tracks plasma membrane-derived endosomes (Vida, 1995). In Col-0 control roots, no GFP signal was detected (Figure 4E), while

analysis of *TTL3-GFP 2.4* revealed the presence of TTL3-GFP in all cell files of the root apical meristem (Figure 4F). Further up, in the meristematic region, TTL3-GFP showed a predominant localization in the outer cell layers (epidermis and cortex) (Figure 4F).

At the subcellular level, TTL3-GFP mostly showed a cytoplasmic localization in the root meristematic cells (Figure 4G). However, we sometimes observed seedlings that, in addition to the cytoplasmic GFP localization, showed GFP signal at the plasma membrane. Quantification of the plasma membrane localization of TTL3-GFP (see Figure legend and Methods section for details) in control growth conditions indicated that in ~30% of the seedlings some cells showed TTL3-GFP localization at the plasma membrane (Figure 4J). Treatment with 1  $\mu$ M eBL, a concentration previously used to analyze short-term BIK1 dynamics (Wang and Chory, 2006), increased the amount of TTL3-GFP protein (Supplemental Figure 12A and 12B) consistent with the increased expression of *TTL3* by BRs. Interestingly, exogenous eBL treatment enhanced the relocalization of TTL3-GFP from the cytoplasm to the plasma membrane (Figure 4H-4J and Supplemental Figure 13A-13B). eBL treatment also caused the appearance of GFP-labeled intracellular structures (Figure 4H). These intracellular TTL3-GFP structures do not colocalize with FM4-64 (Supplemental Figure 13A), eliminating the possibility that they correspond to plasma membrane-derived endosomes, and thus their identity remains elusive.

Consistent with the possibility that the plasma membrane localization of TTL3-GFP in seedlings grown in control medium was caused by endogenous BRs, the percentage of seedlings with plasma membrane signal decreased from ~30% to ~5% after treatment with BRZ (Figure 4K). Further treatment of these seedlings with eBL reverted this effect and increased the plasma membrane localization of TTL3-GFP (Figure 4K).

### **TTL3 associates with the BR signaling components BSK1, BSU1 and BIN2 and directly interacts with BSU1**

Our previous analyses indicate that TTL proteins are required for BR signaling. Considering the structure of these proteins and the interaction of TTL3 with BRI1, one possibility is that these TTL proteins function as a scaffold of additional BR signaling components. We first investigated possible direct interactions between TTL3 and the cytoplasmic BR signaling components BSK1, BSU1 and BIN2, using yeast two-hybrid assays. Using a full-length TTL3 protein, we did not identify interactions with any of the investigated BR components (Figure 5A). However, immunoblot analysis indicated that BD-TTL3 fusion protein was not produced (Supplemental Figure 14), similar to what previously occurred in *E. coli*. Therefore, we generated additional yeast two-hybrid constructs using the TTL3 $\Delta$ N1 and TTL3 $\Delta$ N2 fragments (Figure 1C). As shown in Figure 5A, TTL3 $\Delta$ N1 but not TTL3 $\Delta$ N2 interacted with BSU1, indicating that the six TPR domains

are required for the interaction. In contrast to BSU1, BIN2 and BSK1 did not interact with TTL3 $\Delta$ N1 (Figure 5A). As a control, we used the positive interaction of BIN2 with BSU1 previously described (Kim et al., 2009).

Next, we used Co-IP and BiFC in *N. benthamiana* to investigate possible associations of TTL3 with BSK1, BSU1 and BIN2. TTL3 strongly associates with BSK1 in both Co-IP (Figure 5B) and BiFC assays (Supplemental Figure 6A). BiFC between TTL3 and BSK1 was also obtained when we exchanged nYFP and cYFP tags (Supplemental Figure 6B) and, consistent with the plasma membrane localization of BSK1, the BiFC signal for BSK1-TTL3 was observed at the plasma membrane. TTL3 also associated with BSU1 and BIN2 in both Co-IP and BiFC assays (Figure 5C-5D and Supplemental Figure 6A-6B). Although BSU1 and BIN2 present a dual nuclear and cytoplasmic localization (Maselli et al., 2014; Vert and Chory, 2006), BiFC signals were only observed in the cytoplasm for both TTL3-BSU1 and TTL3-BIN2, which is consistent with the lack of TTL3 protein in the nucleus. A cytoplasmic BiFC signal was also obtained when YFP halves were interchanged among TTL3-BSU1 and TTL3-BIN2 (Figure S2B). Interestingly, we consistently observed that when TTL3 was coexpressed with BIN2 there was a depletion of BIN2 protein amount in the total protein extract (Figure 5D input). This was further quantified using 6 biological replicates confirming that upon TTL3 expression the levels of BIN2 were reduced by approximately 80% (Fig 5E). This was unique for BIN2 since we did not find the same effect with any other protein of the BR pathway (Figure 1E, 5B, 5C) and suggests that TTL3 might function, at least in part, in BR signaling, by negatively regulating the amount of BIN2.

### **TTL3 interacts with the transcription factors BZR1 and affects its cytoplasmic/nuclear localization**

In the absence of BRs, BIN2 phosphorylates and inactivates BZR1 and BES1, which are the two major transcription factors mediating BR-induced transcriptional changes (Belkhadir and Jaillais, 2015). We performed a yeast two-hybrid assay between TTL3 and the transcription factor BZR1 (Figure 6A). As a positive control (Figure 6A), we used the reported interaction between BZR1 with BIN2 (He et al., 2002). As expected, based on the lack of accumulation of the full-length TTL3 protein in yeast (Supplemental Figure 14), no interaction with BZR1 was obtained (Figure 6A). However, we did detect an interaction between TTL3 $\Delta$ N1 and TTL3 $\Delta$ N2 (Figure 1C) and BZR1 (Figure 6A), indicating that the TPR3 to TPR6 region of TTL3 is sufficient for its interaction with BZR1.

TTL3 also associates with BZR1 in Co-IP experiments in *N. benthamiana* (Figure 6B) and in *Arabidopsis* mesophyll protoplasts (Figure 6C). Phosphorylated and dephosphorylated BZR1 proteins show a marked difference in mobility in SDS-PAGE upon expression in *N. benthamiana*

(Figure 6B and Supplemental Figure 15A) and in Arabidopsis protoplasts (Figure 6C) (Gampala et al., 2007; Ryu et al., 2007). Interestingly, only the phosphorylated BZR1 (pBZR1) was co-immunoprecipitated with TTL3 (Figure 6C and Supplemental Figure 15A), suggesting a preferential association of TTL3 with pBZR1. BiFC assays further confirmed the *in vivo* association of BZR1 with TTL3 (Supplemental Figure 6A and 6B). We also observed that while the BiFC signal of TTL3 with plasma membrane BR components results in a smooth YFP fluorescence signal, the BiFC signal of TTL3 with the cytoplasmic components appear punctate (Supplemental Figure 6A and 6B). A similar punctate BiFC signal has been previously reported for BZR1 with BRZ-SENSITIVE-SHORT HYPOCOTYL1 (BSS1) (Shimada et al., 2015) or BES1 with DOMINANT SUPPRESSOR OF KAR 2 (DSK2) (Nolan et al., 2017), although its significance remains unknown.

We then analyzed the effect of TTL3 on the nuclear and cytoplasmic localization of BZR1-GFP. As previously reported, BZR1-GFP in *N. benthamiana* is mainly localized in the nucleus (Figure 6D), while co-expression of BIN2 together with BZR1-GFP promotes its phosphorylation and its cytoplasmic retention (Figure 6D) (Kim et al., 2009). Co-expressing TTL3-HA with BZR1-GFP and BIN2-HA suppressed the cytoplasmic retention of BZR1-GFP promoted by BIN2 (Figure 6D). We also used Arabidopsis plants expressing the salicylate hydroxylase (*NahG*) gene, as these plants are efficiently transiently transformed using *A. tumefaciens* (Rosas-Diaz et al., 2016). Similar to *N. benthamiana*, coexpressing BIN2-HA together with BZR1-GFP increased its cytoplasmic accumulation, which was further abolished by TTL3-HA (Supplemental Figure 15B). This BZR1 nuclear/cytoplasmic localization is associated with the dephosphorylation status of BZR1 (Figure 6E), indicating that TTL3 negatively regulates BIN2 phosphorylation of BZR1 and regulates its activity likely by promoting BIN2 depletion (Figure 5E).

### **TTL3 reinforces BSK1-BZR1 association at the plasma membrane**

The search for BZR1 interacting proteins in Arabidopsis through tandem affinity purification allowed the identification of BSK1 as a BZR1 interactor (Wang et al., 2013), a result that we confirmed using Co-IP (Supplemental Figure 16). This led the authors to suggest that BR-signaling components exist in a multi-protein complex at the plasma membrane. The formation of a multiprotein complex for BR components at the plasma membrane has been recently proposed, with BSK3 (a protein that contain TPR domains) acting as a possible scaffold (Ren et al., 2019). Therefore, we aimed to investigate whether TTL3 could function as an additional scaffold in BR signaling. For this, we determined whether TTL3 expression affects the association at the plasma membrane of BSK1 with cytoplasmic BR components using BiFC. As shown in Figure 7A, a strong BiFC signal was obtained for BSK1 with BRI1, BSU1 and BIN2, while a weak signal was obtained with BZR1. The strong BiFC signal detected for BSK1 with BRI1 and with BSU1 is expected, since

these BR signaling components directly interact with BSK1 (Kim et al., 2009). BIN2, although mainly localizing at the nucleus and cytosol, also localizes at the plasma membrane (Vert and Chory, 2006) and directly interacts with several plasma membrane-localized BSKs (Ren et al., 2019; Sreeramulu et al., 2013). Importantly, the BSK1-BZR1 BiFC signal was strongly enhanced when we co-expressed with TTL3-HA (Figure 7B and 7C), indicating that TTL3 increases the association between BSK1 and BZR1 at the plasma membrane. Further immunoblot analysis confirmed that the increase in BSK1-BZR1 BiFC fluorescence was not due to a differential expression of the BiFC proteins caused by TTL3 expression (Figure 7D).

## DISCUSSION

The expression of *TTL* genes is induced by BRs and TTL3 shows its highest expression at the root elongation zone and at the hypocotyl, areas of high BR activity (González-García et al., 2011; Bernardo-García et al., 2014). Individual *ttl1*, *ttl3*, and *ttl4*, and particularly the triple *ttl134* mutants are hyposensitive to BR in root growth assays and show reduced hypocotyl elongation. Further lines of genetic evidence supporting the function of *TTL* genes in BR signaling come from phenotypic analyses of the quadruple mutants of *ttl* genes with either *bri1-301* or *bes1-D*. At the molecular level, *ttl134* shows increased expression of BR-repressed genes, whereas BR-induced dephosphorylation of the transcription factor BES1 is strongly reduced. At the cellular level, a functional TTL3-GFP shows a dual localization in the cytoplasm and plasma membrane in untreated seedlings. Treatment with eBL caused TTL3-GFP relocalization from the cytoplasm to the plasma membrane, while treatment with a BR biosynthesis inhibitor had the opposite effect. Furthermore, co-expression of TTL3 together with BZR1 and BIN2 abolishes the BIN2-dependent BZR1 cytoplasmic retention in *Arabidopsis* and *N. benthamiana* (Kim et al., 2009; Ryu et al., 2007; Gampala et al., 2007; Tang et al., 2011). Overall, this study reveals that plant-specific TTL proteins function as positive regulators of BR signaling.

TTL proteins contain several defined domains involved in protein-protein interactions and assembly of multiprotein complexes. Consistent with this structure, TTL3 protein associates *in vivo* with all core BR signaling components, with the exception of BAK1, and interacts directly with BRI1, BSU1 and BZR1. Mapping the interaction domains of TTL3 with BRI1 indicates that the last four TPRs are essential for this interaction and that both TRLX and the IDR contribute to strengthen the interaction. The presence of an IDR in TTL proteins can provide additional advantages in their scaffolding and regulatory function since IDRs allow their interaction with a large number of partners due to their ability to adopt different conformations thus allowing the assembly of multiple proteins (Soutourina, 2017). We also found that interaction of TTL3 with

BSU1 requires all 6 TPRs while only the last four TPR domains are required for the interaction with BZR1.

How does TTL function mechanistically in BR signaling? The BR-dependent plasma membrane relocalization of TTL3 probably through interaction with phosphorylated BRI1 and the association with other BR components suggests that these proteins function as a scaffold by bringing them together at the plasma membrane. This is supported by the finding that a weak BZR1 and BSK1 association at the plasma membrane is greatly enhanced by TTL3 overexpression. Our data indicate that TTL3 promotes de-phosphorylation and nuclear localization of BZR1, while TTL3 increased BiFC interaction of BSK1-BZR1 at the plasma membrane. These seemingly contradictory results can be explained by the irreversible assembly of the two YFP halves, an intrinsic feature of BiFC. It is possible that the stability of the BiFC complex formed between BSK1 and BZR1 facilitates the visualization of this likely transient interaction, but will also hinder the dynamics of this protein complex formation (Kudla and Bock, 2016).

Although in current models of BR signaling phosphorylation/de-phosphorylation of transcription factors take place exclusively in the cytoplasm and the nucleus (Belkhadir and Jaillais, 2015; Wang et al., 2012), a survey of the literature provides evidence that the plasma membrane could be an active site of BR signaling, from perception of the hormone to de-phosphorylation of the transcription factors: (1) a significant amount of phosphorylated BZR1 located at the plasma membrane is greatly reduced upon BR treatment (Gampala et al., 2007); (2) BSK1 has been identified as an interactor of BZR1 using non-targeted proteomics, which led the authors to propose that BR-signaling components exist in the plasma membrane as a multi-protein complex (Wang et al., 2013). (3) Several BSKs that are plasma membrane-bound interact with BIN2, suggesting that dephosphorylation of BZR1 and BIN2 is also taking place at the plasma membrane (Maselli et al., 2014; Sreeramulu et al., 2013). In a recent report, BSK3 has been shown to directly interact with BRI1, BSU1, and BIN2 (Ren et al., 2019) and is proposed to function as a scaffold that positively regulates BR signaling by locating BSU1 and BIN2 at the plasma membrane and enhancing their interaction.

The basic function of scaffolding proteins is the assembly of signaling components that enhance the efficiency of the signaling cascade by increasing their local concentrations as well as the localization of the signaling reaction to a specific area of the cell. This could be particularly important in BR signal components because some of these proteins are expressed at vanishingly low levels, like BSU1 and BIN2 (Mora-Garcia, 2004; Peng et al., 2008). This scaffolding function of TTL proteins might also have a role in enhancing signaling specificity by preventing spurious interactions of BR signaling components. This is important because some BR signaling components participate in pathways other than BR. For example, BAK1 and related SERK co-

receptors are involved in numerous responses (Ma et al., 2016) in addition to its role in BR signaling, and BIN2 shows multiple targets that result in different signaling outcomes (Kim et al., 2012; Cai et al., 2014). The importance of scaffold proteins to generate signaling specificity of BIN2 (and related GSK3-like kinases) was recently highlighted by the identification of the plant-specific protein POLAR (Houbaert et al., 2018). POLAR acts in concert with BASL as a stomatal lineage scaffold for GSK3-like kinases that confines them to specific subcellular localizations during stomatal differentiation (Houbaert et al., 2018). Another example is BSK1, which was originally identified in BR signaling by proteomic studies (Tang et al., 2008) but was later found also to regulate immunity (Shi et al., 2013). Because *TTL1*, *TTL3*, and *TTL4* were previously reported to play a role in abiotic stress tolerance and there is increasing evidence for the coordination of BR-promoted growth and abiotic stress responses (Nolan et al., 2017; Zhang et al., 2016; Tian et al., 2018), we cannot exclude that the function of TTL3 (and probably other TTLs) as a scaffold of BR signaling components contribute to this cross-talk.

Our work uncovers TTL proteins as components of BR signaling and places the BR pathway in a spatial context. BSK3 kinase has been shown to function in early BR signaling by acting as a scaffold at the plasma membrane that mediates the assembly of BR components (Ren et al., 2019). Further characterization of these scaffold proteins will reveal how components of the BR cascade are spatially assembled so that their localization and local concentration are controlled for optimal signaling.

# METHODS

## Plant Material

All *Arabidopsis thaliana* plants generated in the present study are of the Columbia-0 ecotype (Col-0). *Arabidopsis* mutants lines used in this study have been previously described: *ttl1* (AT1G53300) Salk\_063943; *ttl2* (AT3G14950) Salk\_106516; *ttl3* (AT2G42580) Sail\_193\_B05; *ttl4* (AT3G58620) Salk\_026396; *ttl134: ttl1 ttl3 ttl4* triple mutant (Lakhssassi et al., 2012); *bak1-4* (SALK\_116202) (Chinchilla et al., 2007); *serk1-1* (SALK\_044330) (Albrecht et al., 2005), *serk1-1 bak1-4* double mutant (obtained by crossing *serk1-1* with *bak1-4*), *bri1-301* (Xu et al., 2008), *ttl134 bri1-301* quadruple mutant (obtained by crossing *ttl134* with *bri1-301*), *bes1-D* (Yin et al., 2002) and *ttl134 bes1-D* quadruple mutant (obtained by crossing *ttl134* with *bes1-D*). Transgenic lines *TTL1p:GUS*; *TTL2p:GUS*; *TTL3p:GUS* and *TTL4p:GUS* (Lakhssassi et al., 2012) were also previously described. Generation of transgenic lines *TTL3-GFP 1.2* (*TTL3p:TTL3g-GFP* line 1.2 in *ttl3* background) and *TTL3-GFP 2.4* (*TTL3p:TTL3g-GFP* line 2.4 in *ttl134* background) is described in the **Generation of Transgenic Plants** section.

## Plant Manipulation and Growth Conditions

*Arabidopsis* standard handling procedures and conditions were employed to promote seed germination and growth. Seeds were surface sterilized and cold treated for three days at 4°C. Then, seeds were sowed onto half-strength Murashige-Skoog agar solidified medium (0.6% (w/v) agar for horizontal growth and 1% (w/v) for vertical growth) containing 1.5% sucrose, unless otherwise stated. Plates were placed either vertically or horizontally in a culture chamber at 22 ± 1°C, under cool white light (120 μmol photon m<sup>-2</sup> s<sup>-1</sup>) with a long-day photoperiod (16-h light/8-h dark cycle) unless otherwise stated. When required, seedlings were transferred to soil after seven days of in vitro growth and watered every two days. In soil, plants were grown in a mixture of organic substrate and vermiculite (4:1 v/v) under controlled conditions: 23 ± 1°C, 16-h light/8-h dark cycle (~120 μmol photon m<sup>-2</sup> s<sup>-1</sup>). Freshly harvested seeds were used for all phenotypic analyses.

## Plasmid Constructs

A genomic fragment spanning the 1.7-kb *TTL3* promoter (*TTL3p*) region upstream of the start codon and the *TTL3* genomic region (*TTL3g*) without stop codon was PCR amplified using the primers detailed in **Supplemental Table 1** and cloned into the pCR8 ENTRY vector (Invitrogen).

The coding DNA sequence (CDS) without the stop codon of *TTL3* and *BSK1*, as well as the CDS with the stop codon of the wild-type BRI1 cytoplasmic domain (residues 814–1196), BRI1

cytoplasmic domain JMCT9D (BRI1<sup>cyt</sup><sup>JMCT9D</sup> residues 250–662), and TTL3 truncated version TTL3ΔN1 (residues 204-691), TTL3ΔN2 (residues 371-691), TTL3ΔN3 (residues 567-691), TTL3ΔC1 (residues 1-306) and TTL3ΔC2 (residues 1-595) was PCR amplified using the primers detailed in **Supplemental Table 1** and cloned into the *pENTR/D-TOPO* vector using the pENTR Directional TOPO cloning kit (Invitrogen). The pUNI51 (Salk Institute) cDNA clone was used as template to PCR amplify the *TTL3* CDS without the stop codon. Total RNA from Arabidopsis Col-0 was used to generate cDNA that was then used as a template to PCR amplify BSK1 CDS without the stop codon. The expression clone pMAC-flag-BRI1-CD-JMCT9D (Wang et al., 2008) was used as template for PCR amplification of BRI1<sup>cyt</sup><sup>JMCT9D</sup> and it was a gift from Xiaofeng Wang (College of Horticulture Northwest, A&F University, Yangling Shaanxi).

pENTR vectors including CDS without the stop codon of *BRI1*, *BAK1*, *BIN2*, *BSU1* and *BZR1*, were obtained by Gateway BP-reaction (Invitrogen) using an expression clone for each gene of interest (containing *attB* sites) and the pDONR/Zeo vector. Expression clones, used as templates for cloning *BRI1*, *BAK1*, and *BZR1* in the pENTR/D-Topo by Gateway BP-reaction, were previously published (Schwessinger et al., 2011; Lozano-Durán et al., 2014). The expression clones used to clone *BSU1* (Mora-Garcia, 2004) and *BIN2* (Bernardo-García et al., 2014) in pENTR/D-Topo by the Gateway BP-reaction were a gift from Santiago Mora Garcia (Fundación Instituto Leloir and IIBBA) and Salomé Prat (CNB-CSIC), respectively.

All the resulting pENTR clones were verified by diagnostic PCR, restriction analysis, and sequencing. These pENTR clones in combination with the appropriate destination vectors (pDEST) were used to create the final Gateway-expression constructs by LR-reaction (Invitrogen). The pETG-30A and pETG-30A vectors were provided by the European Molecular Biology Laboratory (EMBL) and were used as pDEST to generate GST and MBP N-terminus fusion proteins for GST-pull-down assays. The pGWB4, 5, 6 and 14, from the pGWB vector series, were provided by Tsuyoshi Nakagawa (Nakagawa et al., 2007) (Department of Molecular and Functional Genomics, Shimane University), and were used as pDEST for the transient expression in *N. Benthamiana* in the Co-IP and co-expression assays (pGWB5, 6 and 14) or for generating stable transgenic Arabidopsis lines (pGWB4). pDEST-GW-VYNE and pDEST-GW-VYCE (Christian et al., 2009) were used for BiFC assays. The Gateway destination vector pUC19(35S:GW-GFP) and pBSSK(35S:GW-HA) were used to transfect protoplasts for transient expression and Co-IP assays. The pUC19(35S:GW-GFP) vector was provided by José Alonso (Department of Plant and Microbial Biology, North Carolina State University), and contains the pGWB5 cassette between HindIII-SacI restriction sites in the pUC19 vector backbone. The pBSSK(35S:GW-HA) vector was generated in this work by cloning the pGWB14 cassette between HindIII-SacI in the pBSSK vector backbone. The pGADT7(GW) and pGBKT7(GW) destination

vectors were provided by Salomé Prat (CNB-CSIC) and used for yeast two-hybrid assay. All the expression clones were verified by diagnostic PCR and restriction analysis.

## Generation of Transgenic Plants

Expression constructs were transformed into *Agrobacterium tumefaciens* strain GVG3101::pMP90 through electroporation and confirmed by diagnostic PCR. The pGWB4 harboring the *TTL3p:TTL3g-GFP* construct was transformed into *Arabidopsis* plants by floral dip (Clough and Bent, 1998) to generate stable transgenic plants. *TTL3p:TTL3g-GFP* was transformed into both the *ttl3* single mutant and the *ttl134* triple mutant. T3 or T4 homozygous transgenic plants were used in this study.

## Venation pattern phenotype

Cotyledons (embryonic leaves) from two-week-old seedlings were cleared and observed under a Nikon AZ100 Multizoom light microscope to analyze vascular patterning and the percentage of cotyledons displaying each venation pattern categories is depicted in **Supplemental Figure 1**. Approximately 200 cotyledons per genotype were analyzed. Representative images of each observed venation pattern categories were acquired.

For clearing cotyledons, the two-week-old seedlings were immersed sequentially in 50% ethanol for 1 hour, 99% ethanol overnight, and 50% ethanol for 1 hour, and finally transferred to ddH<sub>2</sub>O. Seedlings were mounted on slides in 50% glycerol and visualized under a light microscope or using the Nikon AZ100 Multizoom microscope system as described above.

## Morphological characterization of seedlings

Seedlings were grown vertically in long-day photoperiod for 3 (root analysis) or 7 (hypocotyl analysis) days in half-strength MS agar solidified medium supplemented with 1.5% (w/v) sucrose. The root and hypocotyl length of seedlings grown vertically as described above was measured and the data were analyzed as described in the **Quantification and Statistical Analysis** section.

## BL Sensitivity Determined by Root Growth Inhibition

Two different BR-inhibition root growth assays were performed to measure BR sensitivity.

(1) Seedlings were grown vertically in a long-day photoperiod for 4 or 5 days in half-strength MS agar solidified medium supplemented with 1.5% (w/v) sucrose, and then transferred to half-

strength MS agar solidified medium supplemented with 1.5% (w/v) sucrose containing either mock (eBL solvent as control) or 100 nM eBL (PhytoTechnology Laboratories) and photographed 6 or 8 days later.

(2) Seedlings were grown vertically in a long-day photoperiod for 7 days in half-strength MS agar solidified medium supplemented with 1.5% (w/v) sucrose, containing either mock (eBL solvent as control) or 500 nM eBL (PhytoTechnology Laboratories) and photographed. Root length of seedlings grown for 7 days in the presence of 500 nM of eBL were divided by the mean of root length of seedlings grown for 7 days in the absence of BL to calculate the root length fold change. The eBL (PhytoTechnology Laboratories) was added from a 5 mM stock solution freshly prepared in 80% (v/v) ethanol.

To determine the eBL sensitivity of Col-0 and mutants, the root length of seedlings grown vertically as described above was measured and the data were analyzed as described in the **Quantification and Statistical Analysis** section.

### **BL Sensitivity Determined by Phosphorylation status of BES1**

Seedlings were grown vertically in a long-day photoperiod for 7 days in half-strength MS agar solidified medium supplemented with 1.5% (w/v) sucrose, and then transferred to half-strength MS liquid medium supplemented with 1.5% (w/v) sucrose containing 2.5  $\mu$ M BRZ (TCI Europe) and grown for 3 more days. To determine the eBL sensitivity of Col-0 and *ttl134*, the seedlings were treated with either mock (eBL solvent as control) or 10 nM eBL (PhytoTechnology Laboratories) and frozen in liquid nitrogen after 0, 30 and 60 minutes of treatment. Total protein was extracted as described in **Extraction of Total Protein from Arabidopsis** section and analyzed by immunoblotting using an anti-BES1 antibody (dilution 1:500) (Yu et al., 2011) as described in the **Immunoblot** section.

### **Phenotypic Analysis of Hypocotyl elongation in dark**

Freshly harvested seeds were surface sterilized and cold treated for three days at 4°C. Then, seeds were sowed individually onto half-strength Murashige-Skoog 1% (p/v) agar solidified medium containing 1.5% sucrose for vertical growth. Seedlings were grown for 4 days in long-day photoperiod, and then placed in dark conditions (vertical growth in a culture chamber at 22  $\pm$  1°C). Seedlings were photographed and hypocotyl length was measured 3 days after placing plates in dark conditions.

### **Total RNA Extraction and Quantitative PCR Analysis**

Ten-day-old seedlings (10 seedlings per biological replicate) grown for five days on half-strength

MS agar solidified medium were transferred to half-strength MS liquid medium supplemented with 1% (w/v) sucrose (grown for 5 extra days), and were used for total RNA extraction. Plant tissue was ground to a fine powder in liquid nitrogen. Approximated 100 mg of ground tissue per sample was homogenized in 1 mL of the commercial reagent TRIsure (Bioline), and total RNA was extracted following the manufacturer's instructions. The RNA concentration and purity were determined spectrophotometrically (Nanodrop ND-1000 Spectrophotometer). RNA samples (10 µg per sample) were DNase-treated with Turbo DNA-free DNase (Ambion) and 1 µg of RNA per sample was run on a 1% agarose gel to confirm RNA integrity. First-strand cDNA was synthesized from 1 µg of RNA using the iScript cDNA synthesis kit (BioRad), according to the manufacturer's instructions. cDNAs were amplified in triplicate by quantitative PCR using SsoFast EvaGreen supermix (BioRad) and the MyiQ Thermal cycler (Bio Rad). The relative expression values were determined using *ACTINE 2* as a reference gene and plotted relative to Col-0 expression level. Primers used for quantitative PCR (qPCR) are listed in **Supplemental Table 2**.

### **Transient Expression in *N. benthamiana***

For transient expression in *Nicotiana benthamiana*, *Agrobacterium tumefaciens* (GV3101::pMP90) carrying the different constructs was used together with the p19 strain (Voinnet et al., 2003) for infiltration into 4- to 5-week-old *N. benthamiana* leaves at the abaxial side of the leaf lamina. After infiltration, all plants were kept in the greenhouse and analyzed 2 days later. *Agrobacterium* cultures were grown overnight in LB medium containing rifampicin (50 µg/mL), gentamycin (25 µg/mL) and the construct-specific antibiotic. Cells were then harvested by centrifugation (15 minutes, 3000g in 50 mL falcon tubes) at room temperature, pellets were resuspended in agroinfiltration solution (10 mM morpholineethanesulfonic acid (MES) pH 5.6, 10 mM MgCl<sub>2</sub>, and 1 mM acetosyringone) and incubated for 2 hours in dark conditions at room temperature. For double infiltration experiments, *Agrobacterium* strains were infiltrated at an optical density at 600 (OD<sub>600</sub>) of 0.4 for the constructs and 0.2 for the p19 strain. For triple infiltration experiments, *Agrobacterium* strains were infiltrated at OD<sub>600</sub> of 0.26 for the constructs and at OD<sub>600</sub> of 0.2 for the p19 strain. An *Agrobacterium* strain harboring an empty vector (or GUS-HA expressing vector) was used to obtain a total OD<sub>600</sub> of approximated 1 in all the infiltration experiments.

For eBL treatment analysis, leaves were pre-treated with 5 µM BL for 3 hours prior to sample collection. *N. benthamiana* leaves were infiltrated with water or 5 µM eBL (PhytoTechnology Laboratories) infiltration solution (10 µL eBL 5mM stock solution in 10 mL H<sub>2</sub>O), made from a 5 mM stock solution freshly prepared in 80% (v/v) ethanol.

## Transient Expression in Arabidopsis NahG plants

*Agrobacterium tumefaciens*-mediated expression in Arabidopsis NahG plants (Rosas-Diaz et al., 2016) was performed as described for transient expression in *N. benthamiana* with some modifications. *Agrobacterium* strains were resuspended with an equal OD<sub>600</sub> in infiltration solution to obtain a total OD<sub>600</sub> of 0.05 for injection into the abaxial leaf sides of 4- to 5-week-old Arabidopsis plants. At least 6 plants per co-infiltration mixture and 4 leaves per plant were used per experiment.

## Recombinant Protein Purification and In Vitro Pull-down Assay

The coding sequences of wild-type BRI1 cytoplasmatic domain (residues 814–1196), BRI1 cytoplasmatic domain JMCT9D (residues 250–662), TTL3ΔN1 (residuos 204-691) and TTL3ΔN3 (residues 567-691) were cloned as described in **Plasmid Constructs** section to generate MBP-BRI1cyt, MBP-BRI1cyt<sup>JMCT9D</sup>, GST-TTL3ΔN1 and GST-TTL3ΔN3 constructs. Recombinant proteins were expressed in *E. coli* strain BL21 (DE3) and extracted using Buffer A (140mM NaCl, 2.7mM KCl, 10mM Na<sub>2</sub>HPO<sub>4</sub>, 1.8mM KH<sub>2</sub>PO<sub>4</sub>, 1% Triton X-100, pH 8, supplemented with 1 mM PMSF, 0.2 μL/10 mL of Benzonase Nuclease (Sigma), and 1 mg/mL Lisozyme). MBP and GST fusion proteins were purified with Glutathione Sepharose 4B GST-tagged protein purification resin (GE Healthcare) or MBP binding protein coupled to agarose beads (MBP-Trap\_A, Chromotek), respectively, according to the manufacture's instructions.

To investigate protein-protein interactions, the GST-tagged proteins were first captured by the glutathione agarose-coated beads and then incubated with the MBP-tagged proteins in dilution/wash buffer [50 mM Tris-HCl, pH 7.5; 150 mM NaCl; 10% glycerol; 10 mM EDTA, pH 8; 10 mM DTT; 0,5 mM PMSF; 1% (v/v) P9599 protease inhibitor cocktail (Sigma)] at 4°C for 1 hour in an end-over-end rocker. Protein-protein interaction complexes bound to the glutathione agarose-coated beads were pulled down, washed three times with the dilution/wash buffer and analyzed by immunoblot as described in the **Immunoblot** section.

Immunoblotted GST and MBP-tagged protein were detected using an anti-GST antibody (Sigma-aldrich, Catalog # G7781; Dilution 1:10000) and a specific anti-BRI1 antibody (Bojar et al., 2014) (Dilution 1:2000) as described in the **Immunoblot** section.

## Protein extraction and Co-Immunoprecipitation in *N. benthamiana*

Protein extraction and Co-Immunoprecipitation in *N. benthamiana* were performed as previously described (Kadota et al., 2016) with some modifications. Briefly, four-week-old *N. benthamiana* plants were used for transient expression assays as described in the **Transient expression in *N. benthamiana*** section. Leaves were ground to fine powder in liquid nitrogen. Approximated 0.5g of

ground leaves per sample were used and total proteins were then extracted with extraction buffer [50 mM Tris-HCl, pH 7.5; 150 mM NaCl; 10% glycerol; 10 mM EDTA, pH 8; 1 mM NaF; 1 mM Na<sub>2</sub>MoO<sub>4</sub>·2H<sub>2</sub>O; 10 mM DTT; 0.5 mM PMSF; 1% (v/v) P9599 protease inhibitor cocktail (Sigma); Nonidet P-40, CAS: 9036-19-5 (USB Amersham life science) 0.5% (v/v) for CoIP involving transmembrane proteins BRI1 and BAK1, and 0.2% (v/v) for the rest of CoIP] added at 2 mL/g of powder using an end-over-end rocker for 30 minutes at 4°C. Samples were centrifuged 20 minutes at 4°C and 9000 RPM (9056g). Supernatants (approximated 4 mg/mL protein) were filtered by gravity through Poly-Prep Chromatography Columns (#731-1550 Bio-Rad) and 100 µL was reserved for immunoblot analysis as input. The remaining supernatants were incubated for 2 hours at 4°C with 15 µL GFP-Trap coupled to agarose beads (Chromotek) in an end-over-end rocker. During incubation of protein samples with GFP-Trap beads, the final concentration of detergent (Nonidet P-40) was adjusted to 0.2% (v/v) in all cases to avoid unspecific binding to the matrix as recommended by the manufacturer. Following incubation, the beads were collected and washed four times with the wash buffer (similar to extraction buffer but without detergent). Finally, beads were resuspended in 75 µL of 2x concentrated Laemmli Sample Buffer and heated at 60°C for 30 minutes (for CoIP involving transmembrane proteins BRI1 and BAK1) or (70°C for 20 minutes (for the remaining CoIPs) to dissociate immunocomplexes from the beads. Total (input), immunoprecipitated (IP) and Co-Immunoprecipitated (CoIP) proteins were separated in a 10% SDS-PAGE gel, and analyzed as described in the **Immunoblot** section.

## **Bimolecular Fluorescence Complementation (BiFC) Assays**

Leaves were co-agroinfiltrated as described in the **Agrobacterium-Mediated Transient Expression in *Nicotiana benthamiana*** section with the *Agrobacterium* strain harboring a construct to express a given protein (Protein A) fused to the N-terminus half of YFP (Protein A-nYFP) and the BiFC partner protein (Protein B) fused to the C-terminus half of YFP (Protein B-cYFP), and vice versa (Protein A-cYFP and Protein B-nYFP) to test both BiFC directions. Leaves were observed using a confocal microscope two days after infiltration, as described in **Confocal Imaging of Arabidopsis and *Nicotiana benthamiana*** section.

## **Confocal Imaging of Arabidopsis and *N. benthamiana***

Arabidopsis seedlings were germinated in half-strength Murashige-Skoog agar solidified medium (1% agar (w/v) for vertical growth) supplemented with 1.5% sucrose. For eBL treatment analysis, 4-day-old seedlings were incubated in 2 mL of half-strength Murashige and Skoog medium

supplemented with 1.5% (w/v) sucrose containing either mock (eBL solvent as control) or 1  $\mu$ M eBL (PhytoTechnology Laboratories). For BRZ/eBL treatment analysis, 3-day-old seedlings were incubated in 2 mL of half-strength Murashige and Skoog medium supplemented with 1% (w/v) sucrose, containing either mock (BRZ solvent as control) or 5  $\mu$ M BRZ (TCI Europe) for 12 hours (overnight). The next morning samples were further treated with mock or 1  $\mu$ M eBL (PhytoTechnology Laboratories) for another 1 hour before being analyzed by confocal microscopy. The eBL (PhytoTechnology Laboratories) and BRZ (TCI Europe) were added from a 5 mM stock solution freshly prepared in 80% (v/v) ethanol. For visualization of plasma membrane, seedlings were incubated in 1 mL ddH<sub>2</sub>O containing 1  $\mu$ g/mL FM4-64 (Invitrogen Molecular Probes) prepared from a 1 mg/mL stock solution for 3-4 minutes, rinsed in ddH<sub>2</sub>O to remove the excess stain and visualized under confocal microscopy.

For confocal imaging of *Nicotiana benthamiana* leaves in co-expression and BiFC experiments, GFP or YFP fluorescence of the lower epidermis of the leaf was visualized with the confocal 2 days after infiltration.

Confocal imaging of *Arabidopsis NahG* plants was performed as described for *Nicotiana benthamiana*, but in this case, images are a maximum Z-projection of seven 1  $\mu$ m spaced confocal planes from the cell equatorial plane to the cell surface.

All confocal images were obtained using a Leica TCS SP5 II confocal microscope equipped with a 488-nm argon laser for GFP and YFP, and a 561-nm He-Ne laser for FM4-64. Leica LAS AF Lite platform and the Java-based image-processing program FIJI (Schneider et al., 2012; Schindelin et al., 2012) were used in the processing of all microscopy images.

### **Stereo Microscopy of Arabidopsis Seedlings**

Representative images of *Arabidopsis* seedlings were acquired using the Nikon Eclipse Ti basic Fluorescence Microscope system with a filter for GFP or ZEISS SteREO Discovery V12 with digital cam AxioCam 503 color (excitation wavelengths; 488 and emission wavelengths; 498-550). Wilde-type Col-0 *Arabidopsis* seedlings were used as a negative control for chlorophyll fluorescence.

## GUS Staining Assay

Four-day-old seedlings were transferred to a medium containing 0.2  $\mu\text{M}$  eBL (PhytoTechnology Laboratories) for 24 hours and then stained for GUS activity. Plant tissues were immersed in histochemical GUS staining buffer (100mM  $\text{NaPO}_4$  pH7, 0.5 mM  $\text{K}_3[\text{Fe}(\text{CN})_6]$ , 0.5 mM  $\text{K}_4[\text{Fe}(\text{CN})_6]$ , 20% Methanol, 0.3% Triton X-100 and 2 mM 5-Bromo-4-chloro-3-indoxyl-beta-D-glucuronide cyclohexylammonium (X-gluc) (Gold Biotechnology, USA)) in multi-well plates, vacuum-infiltrated (60 cm Hg) for 10 minutes three times, and then wrapped in aluminum foil and incubated at 37°C for 12 hours. Samples were then washed several times with 95% ethanol until complete tissue clarification, stored in 50% glycerol and photographed using the Nikon AZ100 Multizoom microscope system.

## Protoplast Transient Expression Assays

Protoplast extraction and transfection were performed as previously described (Yoo et al., 2007). Briefly, leaves from 5-week-old *Arabidopsis* Col-0 plants grown under a 10-hour daylight photoperiod were cut into very small strips and digested for 3 hours in the darkness at room temperature. Protoplasts were then washed and resuspended to a concentration of  $5 \times 10^5$  protoplasts/mL before PEG-mediated transfection for 10 minutes. Twenty microliters of plasmid expressing GFP or 100  $\mu\text{L}$  of plasmid expressing TTL3-GFP/BZR1-HA were used to transfect 2 mL protoplasts for each transfection. All the plasmids were used at a concentration of 1  $\mu\text{g}/\mu\text{L}$ . The transfected protoplasts were incubated for 6 hours at room temperature and collected for protein extraction and immunoprecipitation, as described for *N. benthamiana* samples.

## Yeast Two-Hybrid Assay

The Gal4-based yeast two-hybrid system (Clontech Laboratories Inc.) was used for testing the interaction between TTL3 and different components of the brassinosteroid signaling pathway. The bait and prey constructs are explained in the **Plasmid Constructs** section. The bait and prey plasmids were transformed into *Saccharomyces cerevisiae* strain AH109 as previously described (Gietz and Schiestl, 1995) and transformants were grown on plasmid-selective media (SD/-Trp-Leu). Plates were incubated at 28°C for 4 days and independent colonies for each bait-prey combination were resuspended in 200  $\mu\text{L}$  of sterile water. Ten-fold serial dilutions were made and 5  $\mu\text{L}$  of each dilution were spotted onto three alternative interaction-selective medium (SD/-Trp-Leu-His+3-AT (3-amino-1, 2, 4-triazole, 2mM), SD/-Trp-Leu-Ade, and SD/-Trp-Leu-Ade+3-AT). Plates were incubated at 28 °C and photographed 3 or 7 days later.

## Yeast Two-Hybrid Protein Extraction

For immunoblot analysis, one or two independent yeast co-transformants (a and b) for each bait-prey plasmid combination were grown in 50 mL of SD/-Leu-Trp to an OD<sub>600</sub> of 0.7-1. Cultures were centrifuged at 4,000 rpm for 3 minutes. The resulting pellet was washed once with cold water and resuspended in 200 µL of RIPA buffer (2 mM sodium phosphate buffer pH 7, 0,2% Triton X-100, 0.02% -w/v- SDS, 0.2 mM EDTA pH 8, 10 mM ClNa) containing protease inhibitor (1 tablet/10 mL, cOmplete, Mini, EDTA-free Protease Inhibitor Cocktail, Roche). Glass beads (500 µL, 425-600 µm, Sigma) were added and the sample was vortexed in FastPrep™ FP120 (BIO 101) at a power setting of 5.5 for two 15-seconds intervals separated by 1-minute interval on ice. Then 400 µL RIPA buffer with protease inhibitors was added and the sample was vigorously vortexed. The supernatant was recovered, and the protein concentration was determined using Bradford assays. Total protein (50 µg) was resolved on 10% polyacrylamide/SDS gels and analyzed by immunoblotting using an anti-Myc Tag (1:2000, Abgent), which is transcriptionally fused to Gal4BD, as described in the **Immunoblot** section

## Extraction of Total Protein from Arabidopsis

Arabidopsis tissue was ground to a fine powder in liquid nitrogen. Approximately 100 mg of ground tissue per sample was used for total protein extraction. Denatured protein extracts were obtained by homogenizing and incubating plant material in 200 µL of 2X Laemmli buffer [125 mM Tris-HCl pH 6.8; 4% (w/v) SDS; 20% (v/v) Glycerol; 2% (v/v) Beta-mercaptoethanol; 0,01% (w/v); Bromophenol blue] for 5 minutes at 95°C, centrifuged (5 minutes, 20, 000 g) at room temperature and the total proteins from supernatant were separated in a 10% SDS-PAGE gel, and analyzed as described in the **Immunoblot** section.

## Immunoblot

Proteins separated by SDS-PAGE polyacrylamide gel electrophoresis were electroblotted using Trans-blot Turbo Transfer System (BioRAD) onto polyvinylidene difluoride (PVDF) membranes (Immobilon-P; Millipore) following instructions by the manufacturer (preprogramed protocols optimized for the molecular weight of the proteins of interest). PVDF membranes, containing electroblotted proteins, were then incubated with the appropriate primary antibody followed by the appropriate secondary peroxidase-conjugated antibody. In addition to the primary antibodies described in the previous methods section, the following primary antibodies were used for detection of epitope-tagged proteins: mouse monoclonal anti-GFP clone B-2 (1:600; Santa Cruz Biotechnology, Catalog # sc-9996, Lot # C0619), mouse monoclonal anti-HA clone HA-7 (1:3000;

Sigma-Aldrich, Catalog # H3663) and mouse monoclonal anti-myc clone 9E10 (1:2000; Abgent, Catalog # AM1007a). The secondary antibodies used in the present study were: anti-mouse IgG whole molecule–Peroxidase (1:80000; Sigma-Aldrich, Catalog # A9044, Lot # 031M4752) and anti-rabbit IgG whole molecule–Peroxidase (1:80000; Sigma-Aldrich, Catalog # A0545, Lot # 026M4782V).

Proteins and epitope-tagged proteins on immunoblots were detected using the Clarity ECL Western Blotting Substrate or SuperSignal West Femto Maximum Sensitivity Substrate according to the manufacturer's instructions, and images of different time exposures were acquired using the Chemidoc XRS+System (Biorad). SDS-PAGE polyacrylamide gels and immunoblotted PVDF membranes were stained with Coomassie blue to confirm equal loading of the different samples in a given experiment.

## **QUANTIFICATION AND STATISTICAL ANALYSIS**

### **Arabidopsis eFP Browser Data Analysis**

Gene expression level data from hormone responses were retrieved from the Arabidopsis eFP Browser (Hormone Series) website (<http://bar.utoronto.ca/efp/cgi-bin/efpWeb.cgi>; Winter et al., 2007). Data used for the analysis was obtained from 7-day-old wild-type seedlings. Differential expression was calculated by dividing the expression value of each gene in a given hormone treatment by the corresponding mock control (fold-change of hormone treatment relative to the mock). The hormone gene expression response was calculated and the heatmap was created using Microsoft Office Excel (Microsoft). In the heatmap, red represents induction and blue represents repression as response to the indicated hormone.

### **Quantification of Fluorescent Protein Signal**

For quantification of fluorescent protein signal in plasma membrane vs cytoplasm, all images were analyzed using FIJI software (Schindelin et al., 2012; Schneider et al., 2012). To measure the ratio between nuclear and cytoplasmic signals, a small area of fixed size (8 pixels) was drawn, and measurements of integrated densities were taken from representative areas within the plasma membrane and cytoplasm of each cell. To delineate the plasma membrane area, FM4-64 was used to stain the cells. Average ratios between plasma membrane and cytoplasmic signal intensities were calculated based on measurements from 3 cells per plant. n=10 plants analyzed (3 cells per plant). This experiment was repeated twice with similar results.

Additionally, for quantification of fluorescent protein signal, line scan measurements spanning membrane and cytoplasm were carried out from images using FIJI (Schindelin et al., 2012;

Schneider et al., 2012) software, and representative plot profiles of sample measurements are presented in **Figure 4I**.

The quantification the BiFC fluorescence intensity of BSK1 and BZR1 in the presence or absence of TTL3-HA (Figure 7B) was performed using FIJI software (Schindelin et al., 2012; Schneider et al., 2012). The area in pixels and raw integrated density of the fluorescence signal were measured in at least 5 randomly chosen regions of infiltrated leaves per experiment. Fluorescence Intensity (Arbitrary Units, a.u.) was calculated by dividing the raw integrated density by the area in pixels of the fluorescence signal.

## Statistics

Band intensity quantification of protein signal detected by immunoblot, integrated densities from representative areas within the plasma membrane and cytoplasm of each cell analyzed by confocal imaging, as well as Arabidopsis root and hypocotyl lengths were measured from images using FIJI (Schindelin et al., 2012; Schneider et al., 2012) software. The data for qRT-PCR were gathered with MyiQ optical system software (Bio Rad). For statistical analysis unpaired t-test or one-way ANOVA followed by Tukey's multiple comparison test ( $p < 0.05$ ) was performed using GraphPad Prism version 6.00 for Mac (GraphPad Software, La Jolla California USA, [www.graphpad.com](http://www.graphpad.com)). ANOVA and/or T-test results for the data presented in each figure are detailed in the **Supplemental Data Set 1**. Asterisks indicate statistical differences between mutant vs Col-0, unless otherwise specified, as determined by the unpaired *t-test* (\*  $P \leq 0.05$ , \*\*  $P \leq 0.01$ , \*\*\*  $P \leq 0.001$  \*\*\*\*  $P \leq 0.0001$ ). Different lowercase letters in the graphs indicate significant differences. Data represent mean values and error bars are SEM. In figure legends, n means number of plants for phenotypic analysis, numbers of biological replicates (3 technical replicates per biological replicate) for qPCR analysis, or number of cells (3 independent measurements performed per cell) analyzed for quantification of fluorescent protein signal in plasma membrane vs cytoplasm. The experiments were repeated at least three times with similar results.

## ***In silico* Three-Dimensional Structural Model of TTL3**

The *in silico* protein structure prediction for TTL3 protein was built by submitting primary sequences to the I-TASSER server (Zhang, 2008) and processed by PyMOL (Schrödinger). Intrinsically disordered regions (IDRs) were predicted using GlobPlot 2, available at <http://globplot.embl.de/>. Tetratricopeptide Repeat (TPR) and thioredoxin-like (TPRX) domains were predicted using the SMART/Pfam server and were previously described (Lakhssassi et al., 2012).

## Accession Numbers

Sequence data from this article can be found in the EMBL/GenBank data libraries under accession numbers: *AT1G53300* for *TTL1*, *AT3G14950* for *TTL2*, *AT2G42580* for *TTL3*, *AT3G58620* for *TTL4*, *AT4G33430* for *BAK1*, *AT1G71830* for *SERK1*, *AT4G39400* for *BRI1*, *AT2G01950* for *BRL2*, *AT4G35230* for *BSK1*, *AT1G03445* for *BSU1*, *AT4G18710* for *BIN2*, *AT1G75080* for *BZR1*, *AT1G19350* for *BES1*.

## Supplemental Data

**Supplemental Figure 1.** *TTL* genes are required for cotyledon vein pattern formation. Supports Figure 1.

**Supplemental Figure 2.** *TTL3* presents an intrinsically disorder region (IDR) at the N-terminus. Supports Figure 1.

**Supplemental Figure 3.** Protein sequence alignment of *BRI1* and *BRL2* cytoplasmic domain. Supports Figure 1.

**Supplemental Figure 4.** Purified GST and MBP-fused proteins used for the GST Pull-down assays. Supports Figure 1.

**Supplemental Figure 5.** *TTL3* specifically associates with *BRI1* but not with *BAK1* or free GFP. Supports Figure 1.

**Supplemental Figure 6.** *TTL3* associates with *BSK1*, *BSU1*, *BIN2* and *BZR1* in BiFC experiments. Supports Figure 1, 5 and 6.

**Supplemental Figure 7.** The expression of *TTL1*, *TTL3*, and *TTL4* are specifically induced by BRs. Supports Figure 2 and 3.

**Supplemental Figure 8.** *TTL1*, *TTL3* and *TTL4* genes play a positive role in BR signaling. Supports Figure 2.

**Supplemental Figure 9.** Mutations in *TTL1*, *TTL3* and *TTL4* aggravate the weak *bri1-301* phenotype and alleviate part of the *bes1-D* phenotypes. Supports Figure 3.

**Supplemental Figure 10.** TTL3 presents a cytoplasmic/plasma membrane sub-cellular localization. Supports Figure 4.

**Supplemental Figure 11.** *TTL3-GFP* 1.2 complements the root length phenotype of *ttl3* in response to eBL treatment. Supports Figure 4.

**Supplemental Figure 12.** Immunoblot analyses reveal that eBL treatment induces TTL3-GFP protein stabilization, and that there are no degradation-products of TTL3-GFP in the Arabidopsis TTL3-GFP 2.4 line. Supports Figure 4.

**Supplemental Figure 13.** BRs regulate the cytoplasmic/plasma membrane localization of TTL3. Supports Figure 4.

**Supplemental Figure 14.** TTL3 N-terminus negatively affects the stabilization of TTL3 in yeast heterologous system. Supports Figure 5 and 6.

**Supplemental Figure 15.** TTL3 preferentially associates with the phosphorylated form of BZR1 by Co-IP and regulates its cytoplasmic/nuclear localization. Supports Figure 6.

**Supplemental Figure 16.** BSK1 co-immunoprecipitates with BZR1. Supports Figure 7.

**Supplemental Table 1.** List and description of primers used for cloning into pENTR.

**Supplemental Table 2.** List of primers used for quantitative RT-PCR.

**Supplemental Dataset 1.** Statistical report of t-tests and ANOVAs results for the data presented in each figure.

## **Acknowledgements**

This work was supported by the Ministerio de Economía y Competitividad (cofinanced by the European Regional Development Fund; grant no. BIO2017-82609-R to M.A.B) and by a Formación del Personal Investigador Fellowship from the Ministerio de Economía y

Competitividad (FPI-BES 2015-071256 to A.G-M), by the Shanghai Center for Plant Stress Biology (Chinese Academy of Sciences) and the Chinese 1000 Talents Program (to A.P.M.), and by the Gatsby Charitable Foundation and the European Research Council under the Grant Agreement 309858 (grant “PHOSPHinnATE”) (to C.Z.). D.P. was supported by the Ramón y Cajal program (RYC-2013-12699 MINECO- Universidad de Málaga, Spain). N.L. was supported by a fellowship from Agencia Española de Cooperación Internacional para el Desarrollo (Ministerio de Asuntos Exteriores y Cooperación) and by Ministerio de Educación y Ciencia (Universidad de Málaga, Spain).

We thank Yanhai Yin and Michael Hothorn for generously providing the anti-BES1 and the anti-BRI1 antibodies, respectively.

We are grateful to Salomé Prat (*BIN2* expression clone), Santiago Mora Garcia (BSU1 expression clone), José Alonso (GFP-tagged GW vector for expression in protoplasts) and Xiaofeng Wang (pMAC-flag-BRI1-CD-JMCT9D, BRI1 phosphomimetic mutant) for providing expression clones and vectors used in the present study.

### **Author contributions**

All authors designed the experiments. V.A-S., A.G-M., A.C., N.L., J.P-S., Y.L., A.E-V., D.P., J.P-R., and A.P.M. performed the experiments and analyzed the data. V.A-S., A.P.M., and M.A.B. wrote the manuscript. All authors commented on the manuscript.

### **Competing interests**

I declare that the authors have no financial and non-financial competing interests, or other interests that might be perceived to influence the results and/or discussion reported in this paper.

## REFERENCES

- Albrecht, C., Russinova, E., Hecht, V., Baaijens, E., and de Vries, S. (2005). The Arabidopsis thaliana SOMATIC EMBRYOGENESIS RECEPTOR-LIKE KINASES1 and 2 control male sporogenesis. *Plant Cell* 17: 3337–3349.
- Belkhadir, Y. and Jaillais, Y. (2015). The molecular circuitry of brassinosteroid signaling. *New Phytol.* 206: 522–540.
- Bernardo-García, S., de Lucas, M., Martínez, C., Espinosa-Ruiz, A., Davière, J.-M., and Prat, S. (2014). BR-dependent phosphorylation modulates PIF4 transcriptional activity and shapes diurnal hypocotyl growth. *Genes Dev.* 28: 1681–1694.
- Blatch, G.L. and Lässle, M. (1999). The tetratricopeptide repeat: a structural motif mediating protein-protein interactions - Blatch - 1999 - BioEssays - Wiley Online Library. *Bioessays*.
- Bojar, D., Martinez, J., Santiago, J., Rybin, V., Bayliss, R., and Hothorn, M. (2014). Crystal structures of the phosphorylated BRI1 kinase domain and implications for brassinosteroid signal initiation. *Plant J* 78: 31–43.
- Cai, Z., Liu, J., Wang, H., Yang, C., Chen, Y., Li, Y., Pan, S., Dong, R., Tang, G., Barajas-Lopez, J. de D., Fujii, H., and Wang, X. (2014). GSK3-like kinases positively modulate abscisic acid signaling through phosphorylating subgroup III SnRK2s in Arabidopsis. *Proc. Natl. Acad. Sci. U.S.A.* 111: 9651–9656.
- Caño-Delgado, A., Yin, Y., Yu, C., Vafeados, D., Mora-García, S., Cheng, J.-C., Nam, K.H., Li, J., and Chory, J. (2004). BRL1 and BRL3 are novel brassinosteroid receptors that function in vascular differentiation in Arabidopsis. *Development* 131: 5341–5351.
- Ceserani, T., Trofka, A., Gandotra, N., and Nelson, T. (2009). VH1/BRL2 receptor-like kinase interacts with vascular-specific adaptor proteins VIT and VIK to influence leaf venation. *The Plant Journal* 57: 1000–1014.
- Chaiwanon, J., Wang, W., Zhu, J.-Y., Oh, E., and Wang, Z.-Y. (2016). Information Integration and Communication in Plant Growth Regulation. *Cell* 164: 1257–1268.
- Chinchilla, D., Zipfel, C., Robatzek, S., Kemmerling, B., Nürnberger, T., Jones, J.D.G., Felix, G., and Boller, T. (2007). A flagellin-induced complex of the receptor FLS2 and BAK1 initiates plant defence. *Nature* 448: 497–500.
- Christian, G., Rainer, W., rg, K.J., Ralf-R, M., and Robert, H.N. (2009). New GATEWAY vectors for High Throughput Analyses of Protein–Protein Interactions by Bimolecular Fluorescence Complementation. *Mol Plant* 2: 1051–1058.
- Chung, Y. and Choe, S. (2013). The Regulation of Brassinosteroid Biosynthesis in Arabidopsis. *Critical Reviews in Plant Sciences* 32: 396–410.
- Clough, S.J. and Bent, A.F. (1998). Floral dip: a simplified method for Agrobacterium-mediated transformation of Arabidopsis thaliana. *Plant J* 16: 735–743.
- D'Andrea, L.D. and Regan, L. (2003). TPR proteins: the versatile helix. *Trends Biochem Sci* 28: 655–662.
- Du, J., Yin, H., Zhang, S., Wei, Z., Zhao, B., Zhang, J., Gou, X., Lin, H., and Li, J. (2012). Somatic Embryogenesis Receptor Kinases Control Root Development Mainly via Brassinosteroid-Independent Actions in Arabidopsis thaliana. *J Integrative Plant Biology* 54: 388–399.

- Fàbregas, N., Li, N., Boeren, S., Nash, T.E., Goshe, M.B., Clouse, S.D., de Vries, S., and Caño-Delgado, A.I. (2013). The brassinosteroid insensitive1-like3 signalosome complex regulates Arabidopsis root development. *Plant Cell* 25: 3377–3388.
- Gampala, S.S. et al. (2007). An essential role for 14-3-3 proteins in brassinosteroid signal transduction in Arabidopsis. *Dev. Cell* 13: 177–189.
- Geldner, N., Hyman, D.L., Wang, X., Schumacher, K., and Chory, J. (2007). Endosomal signaling of plant steroid receptor kinase BRI1. *Genes Dev.* 21: 1598–1602.
- Gietz, R.D. and Schiestl, R.H. (1995). Transforming yeast with DNA.(Invited chapter). *Method Mol. Cell. Biol* 5: 255–269.
- González-García, M.-P., Vilarrasa-Blasi, J., Zhiponova, M., Divol, F., Mora-García, S., Russinova, E., and Caño-Delgado, A.I. (2011). Brassinosteroids control meristem size by promoting cell cycle progression in Arabidopsis roots. *Development* 138: 849–859.
- Gou, X., Yin, H., He, K., Du, J., Yi, J., Xu, S., Lin, H., Clouse, S.D., and Li, J. (2012). Genetic evidence for an indispensable role of somatic embryogenesis receptor kinases in brassinosteroid signaling. *PLoS Genet* 8: e1002452.
- Habchi, J., Tompa, P., Longhi, S., and Uversky, V.N. (2014). Introducing Protein Intrinsic Disorder. *Chem. Rev.* 114: 6561–6588.
- He, J.X., Gendron, J.M., Yang, Y., Li, J., and Wang, Z.Y. (2002). The GSK3-like kinase BIN2 phosphorylates and destabilizes BZR1, a positive regulator of the brassinosteroid signaling pathway in Arabidopsis. *Proc. Natl. Acad. Sci. U.S.A.* 99: 10185–10190.
- He, K., Gou, X., Yuan, T., Lin, H., Asami, T., Yoshida, S., Russell, S.D., and Li, J. (2007). BAK1 and BKK1 regulate brassinosteroid-dependent growth and brassinosteroid-independent cell-death pathways. *CURBIO* 17: 1109–1115.
- Houbaert, A. et al. (2018). POLAR-guided signalling complex assembly and localization drive asymmetric cell division. *Nature*: 1–24.
- Jaillais, Y. and Vert, G. (2016). Brassinosteroid signaling and BRI1 dynamics went underground. *Curr. Opin. Plant Biol.* 33: 92–100.
- Kadota, Y., Macho, A.P., and Zipfel, C. (2016). Immunoprecipitation of Plasma Membrane Receptor-Like Kinases for Identification of Phosphorylation Sites and Associated Proteins. In *Methods in Molecular Biology, Methods in Molecular Biology*. (Springer New York: New York, NY), pp. 133–144.
- Kim, T.-W. and Wang, Z.-Y. (2010). Brassinosteroid Signal Transduction from Receptor Kinases to Transcription Factors. *Annu. Rev. Plant Biol.* 61: 681–704.
- Kim, T.-W., Guan, S., Sun, Y., Deng, Z., Tang, W., Shang, J.-X., Sun, Y., Burlingame, A.L., and Wang, Z.-Y. (2009). Brassinosteroid signal transduction from cell-surface receptor kinases to nuclear transcription factors. *Nat. Cell Biol.* 11: 1254–1260.
- Kim, T.-W., Michniewicz, M., Bergmann, D.C., and Wang, Z.-Y. (2012). Brassinosteroid regulates stomatal development by GSK3-mediated inhibition of a MAPK pathway. *Nature* 482: 419–422.
- Kudla, J. and Bock, R. (2016). Lighting the Way to Protein-Protein Interactions: Recommendations on Best Practices for Bimolecular Fluorescence Complementation Analyses. *THE PLANT CELL ONLINE* 28: 1002–1008.

- Lachowiec, J., Lemus, T., Thomas, J.H., Murphy, P.J.M., Nemhauser, J.L., and Queitsch, C. (2013). The protein chaperone HSP90 can facilitate the divergence of gene duplicates. *Genetics* 193: 1269–1277.
- Lakhssassi, N., Doblaz, V.G., Rosado, A., del Valle, A.E., Posé, D., Jimenez, A.J., Castillo, A.G., Valpuesta, V., Borsani, O., and Botella, M.A. (2012). The Arabidopsis tetratricopeptide thioredoxin-like gene family is required for osmotic stress tolerance and male sporogenesis. *Plant Physiol.* 158: 1252–1266.
- Li, J., Wen, J., Lease, K.A., Doke, J.T., Tax, F.E., and Walker, J.C. (2002). BAK1, an Arabidopsis LRR receptor-like protein kinase, interacts with BRI1 and modulates brassinosteroid signaling. *Cell* 110: 213–222.
- Lin, W., Lu, D., Gao, X., Jiang, S., Ma, X., Wang, Z., Mengiste, T., He, P., and Shan, L. (2013). Inverse modulation of plant immune and brassinosteroid signaling pathways by the receptor-like cytoplasmic kinase BIK1. *Proc. Natl. Acad. Sci. U.S.A.* 110: 12114–12119.
- Lozano-Durán, R. and Zipfel, C. (2015). Trade-off between growth and immunity: role of brassinosteroids. *Trends Plant Sci.* 20: 12–19.
- Lozano-Durán, R., Bourdais, G., He, S.Y., and Robatzek, S. (2014). The bacterial effector HopM1 suppresses PAMP-triggered oxidative burst and stomatal immunity. *New Phytol.* 202: 259–269.
- Ma, X., Xu, G., He, P., and Shan, L. (2016). SERKing Coreceptors for Receptors. *Trends Plant Sci.* 21: 1017–1033.
- Maselli, G.A., Slamovits, C.H., Bianchi, J.I., Vilarrasa-Blasi, J., Caño-Delgado, A.I., and Mora-García, S. (2014). Revisiting the evolutionary history and roles of protein phosphatases with Kelch-like domains in plants. *Plant Physiol.* 164: 1527–1541.
- McKinney, E.C. and Meagher, R.B. (1998). Members of the Arabidopsis actin gene family are widely dispersed in the genome. *Genetics* 149: 663–675.
- Mora-Garcia, S. (2004). Nuclear protein phosphatases with Kelch-repeat domains modulate the response to brassinosteroids in Arabidopsis. *Genes Dev.* 18: 448–460.
- Nakagawa, T., Kurose, T., Hino, T., Tanaka, K., Kawamukai, M., Niwa, Y., Toyooka, K., Matsuoka, K., Jinbo, T., and Kimura, T. (2007). Development of series of gateway binary vectors, pGWBs, for realizing efficient construction of fusion genes for plant transformation. *J. Biosci. Bioeng.* 104: 34–41.
- Nam, K.H. and Li, J. (2002). BRI1/BAK1, a receptor kinase pair mediating brassinosteroid signaling. *Cell* 110: 203–212.
- Nolan, T.M., Brennan, B., Yang, M., Chen, J., Zhang, M., Li, Z., Wang, X., Bassham, D.C., Walley, J., and Yin, Y. (2017). Selective Autophagy of BES1 Mediated by DSK2 Balances Plant Growth and Survival. *Dev. Cell* 41: 33–46.e7.
- Peng, P., Yan, Z., Zhu, Y., and Li, J. (2008). Regulation of the Arabidopsis GSK3-like kinase BRASSINOSTEROID-INSENSITIVE 2 through proteasome-mediated protein degradation. *Mol Plant* 1: 338–346.
- Prasad, B.D., Goel, S., and Krishna, P. (2010). In silico identification of carboxylate clamp type tetratricopeptide repeat proteins in Arabidopsis and rice as putative co-chaperones of Hsp90/Hsp70. *PLoS ONE* 5: e12761.

- Ren, H., Willige, B.C., Jaillais, Y., Geng, S., Park, M.Y., Gray, W.M., and Chory, J. (2019). BRASSINOSTEROID-SIGNALING KINASE 3, a plasma membrane-associated scaffold protein involved in early brassinosteroid signaling. *PLoS Genet* 15: e1007904.
- Rosado, A., Schapire, A.L., Bressan, R.A., Harfouche, A.L., Hasegawa, P.M., Valpuesta, V., and Botella, M.A. (2006). The Arabidopsis tetratricopeptide repeat-containing protein TTL1 is required for osmotic stress responses and abscisic acid sensitivity. *Plant Physiol.* 142: 1113–1126.
- Rosas-Diaz, T., Cana-Quijada, P., Amorim-Silva, V., Botella, M.A., Lozano-Durán, R., and Bejarano, E.R. (2016). Arabidopsis NahG plants as a suitable and efficient system for transient expression using *Agrobacterium tumefaciens*. *Mol Plant*.
- Ryu, H., Kim, K., Cho, H., Park, J., Choe, S., and Hwang, I. (2007). Nucleocytoplasmic shuttling of BZR1 mediated by phosphorylation is essential in Arabidopsis brassinosteroid signaling. *Plant Cell* 19: 2749–2762.
- Samakovli, D., Margaritopoulou, T., Prassinos, C., Milioni, D., and Hatzopoulos, P. (2014). Brassinosteroid nuclear signaling recruits HSP90 activity. *New Phytol.* 203: 743–757.
- Schindelin, J. et al. (2012). Fiji: an open-source platform for biological-image analysis. *Nat. Methods* 9: 676–682.
- Schneider, C.A., Rasband, W.S., and Eliceiri, K.W. (2012). NIH Image to ImageJ: 25 years of image analysis. *Nat. Methods* 9: 671–675.
- Schwessinger, B., Roux, M., Kadota, Y., Ntoukakis, V., Sklenar, J., Jones, A., and Zipfel, C. (2011). Phosphorylation-Dependent Differential Regulation of Plant Growth, Cell Death, and Innate Immunity by the Regulatory Receptor-Like Kinase BAK1. *PLoS Genet* 7: e1002046.
- Shi, H., Shen, Q., Qi, Y., Yan, H., Nie, H., Chen, Y., Zhao, T., Katagiri, F., and Tang, D. (2013). BR-SIGNALING KINASE1 Physically Associates with FLAGELLIN SENSING2 and Regulates Plant Innate Immunity in Arabidopsis. *THE PLANT CELL ONLINE* 25: 1143–1157.
- Shigeta, T., Zaizen, Y., Asami, T., Yoshida, S., Nakamura, Y., Okamoto, S., Matsuo, T., and Sugimoto, Y. (2014). Molecular evidence of the involvement of heat shock protein 90 in brassinosteroid signaling in Arabidopsis T87 cultured cells. *Plant Cell Rep.* 33: 499–510.
- Shigeta, T., Zaizen, Y., Sugimoto, Y., Nakamura, Y., Matsuo, T., and Okamoto, S. (2015). Heat shock protein 90 acts in brassinosteroid signaling through interaction with BES1/BZR1 transcription factor. *J. Plant Physiol.* 178: 69–73.
- Shimada, S., Komatsu, T., Yamagami, A., Nakazawa, M., Matsui, M., Kawaide, H., Natsume, M., Osada, H., Asami, T., and Nakano, T. (2015). Formation and dissociation of the BSS1 protein complex regulates plant development via brassinosteroid signaling. *THE PLANT CELL ONLINE* 27: 375–390.
- Soutourina, J. (2017). Transcription regulation by the Mediator complex. *Nature Publishing Group*: 1–13.
- Sreeramulu, S., Mostizky, Y., Sunitha, S., Shani, E., Nahum, H., Salomon, D., Hayun, L.B., Gruetter, C., Rauh, D., Ori, N., and Sessa, G. (2013). BSKs are partially redundant positive regulators of brassinosteroid signaling in Arabidopsis. *Plant J* 74: 905–919.
- Tanaka, K., Asami, T., Yoshida, S., Nakamura, Y., Matsuo, T., and Okamoto, S. (2005). Brassinosteroid homeostasis in Arabidopsis is ensured by feedback expressions of multiple genes involved in its metabolism. *Plant Physiol.* 138: 1117–1125.

- Tang, W. et al. (2011). PP2A activates brassinosteroid-responsive gene expression and plant growth by dephosphorylating BZR1. *Nat. Cell Biol.* 13: 124–131.
- Tang, W., Kim, T.-W., Oses-Prieto, J.A., Sun, Y., Deng, Z., Zhu, S., Wang, R., Burlingame, A.L., and Wang, Z.-Y. (2008). BSKs mediate signal transduction from the receptor kinase BRI1 in *Arabidopsis*. *Science* 321: 557–560.
- Tian, Y. et al. (2018). Hydrogen peroxide positively regulates brassinosteroid signaling through oxidation of the BRASSINAZOLE-RESISTANT1 transcription factor. *Nat Commun* 9: 1063–13.
- van Esse, W., van Mourik, S., Albrecht, C., van Leeuwen, J., and de Vries, S. (2013). A Mathematical Model for the Coreceptors SOMATIC EMBRYOGENESIS RECEPTOR-LIKE KINASE1 and SOMATIC EMBRYOGENESIS RECEPTOR-LIKE KINASE3 in BRASSINOSTEROID INSENSITIVE1-Mediated Signaling. *Plant Physiol.* 163: 1472–1481.
- Vert, G. and Chory, J. (2006). Downstream nuclear events in brassinosteroid signalling. *Nature* 441: 96–100.
- Vida, T.A. (1995). A new vital stain for visualizing vacuolar membrane dynamics and endocytosis in yeast. *The Journal of Cell Biology* 128: 779–792.
- Voinnet, O., Rivas, S., Mestre, P., and Baulcombe, D. (2003). An enhanced transient expression system in plants based on suppression of gene silencing by the p19 protein of tomato bushy stunt virus. *Plant J* 33: 949–956.
- Vriet, C., Russinova, E., and Reuzeau, C. (2013). From squalene to brassinolide: the steroid metabolic and signaling pathways across the plant kingdom. *Mol Plant* 6: 1738–1757.
- Wang, C. et al. (2013). Identification of BZR1-interacting proteins as potential components of the brassinosteroid signaling pathway in *Arabidopsis* through tandem affinity purification. *Mol. Cell Proteomics* 12: 3653–3665.
- Wang, R., Liu, M., Yuan, M., Oses-Prieto, J.A., Cai, X., Sun, Y., Burlingame, A.L., Wang, Z.-Y., and Tang, W. (2016). The Brassinosteroid-Activated BRI1 Receptor Kinase Is Switched off by Dephosphorylation Mediated by Cytoplasm-Localized PP2A B' Subunits. *Mol Plant* 9: 148–157.
- Wang, W., Bai, M.-Y., and Wang, Z.-Y. (2014). The brassinosteroid signaling network—a paradigm of signal integration. *Curr. Opin. Plant Biol.* 21: 147–153.
- Wang, X. and Chory, J. (2006). Brassinosteroids regulate dissociation of BKI1, a negative regulator of BRI1 signaling, from the plasma membrane. *Science* 313: 1118–1122.
- Wang, X., Kota, U., He, K., Blackburn, K., Li, J., and Goshe, M.B. (2008). Sequential Transphosphorylation of the BRI1/BAK1 Receptor Kinase Complex Impacts Early Events in Brassinosteroid Signaling - ScienceDirect. *Dev. Cell.*
- Wang, Z.-Y., Bai, M.-Y., Oh, E., and Zhu, J.-Y. (2012). Brassinosteroid signaling network and regulation of photomorphogenesis. *Annu. Rev. Genet.* 46: 701–724.
- Wilma van Esse, G., Westphal, A.H., Surendran, R.P., Albrecht, C., van Veen, B., Borst, J.W., and de Vries, S.C. (2011). Quantification of the brassinosteroid insensitive1 receptor in planta. *Plant Physiol.* 156: 1691–1700.
- Winter, D., Vinegar, B., Nahal, H., Ammar, R., Wilson, G.V., and Provart, N.J. (2007). An “Electronic Fluorescent Pictograph” browser for exploring and analyzing large-scale biological data sets. *PLoS ONE* 2: e718.

- Xu, W., Huang, J., Li, B., Li, J., and Wang, Y. (2008). Is kinase activity essential for biological functions of BRI1? *Cell Res* 18: 472–478.
- Yang, C.-J., Zhang, C., Lu, Y.-N., Jin, J.-Q., and Wang, X.-L. (2011). The mechanisms of brassinosteroids' action: from signal transduction to plant development. *Mol Plant* 4: 588–600.
- Yang, J., Roe, S.M., Cliff, M.J., Williams, M.A., Ladbury, J.E., Cohen, P.T.W., and Barford, D. (2005). Molecular basis for TPR domain-mediated regulation of protein phosphatase 5. *EMBO J* 24: 1–10.
- Yin, Y., Wang, Z.-Y., Mora-García, S., Li, J., Yoshida, S., Asami, T., and Chory, J. (2002). BES1 accumulates in the nucleus in response to brassinosteroids to regulate gene expression and promote stem elongation. *Cell* 109: 181–191.
- Yoo, S.-D., Cho, Y.-H., and Sheen, J. (2007). Arabidopsis mesophyll protoplasts: a versatile cell system for transient gene expression analysis. *Nat Protoc* 2: 1565–1572.
- Yu, X., Li, L., Zola, J., Aluru, M., Ye, H., Foudree, A., Guo, H., Anderson, S., Aluru, S., Liu, P., Rodermel, S., and Yin, Y. (2011). A brassinosteroid transcriptional network revealed by genome-wide identification of BES1 target genes in *Arabidopsis thaliana*. *Plant J* 65: 634–646.
- Zhang, Y. (2008). I-TASSER server for protein 3D structure prediction. *BMC Bioinformatics* 9: 40.
- Zhang, Y., Liu, Z., Wang, J., Chen, Y., Bi, Y., and He, J. (2015). Brassinosteroid is required for sugar promotion of hypocotyl elongation in *Arabidopsis* in darkness. *Planta* 242: 881–893.
- Zhang, Z., Zhu, J.-Y., Roh, J., Marchive, C., Kim, S.-K., Meyer, C., Sun, Y., Wang, W., and Wang, Z.-Y. (2016). TOR Signaling Promotes Accumulation of BZR1 to Balance Growth with Carbon Availability in *Arabidopsis*. *Curr. Biol.* 26: 1854–1860.
- Zhu, J.-Y., Li, Y., Cao, D.-M., Yang, H., Oh, E., Bi, Y., Zhu, S., and Wang, Z.-Y. (2017). The F-box Protein KIB1 Mediates Brassinosteroid- Induced Inactivation and Degradation of GSK3-like Kinases in *Arabidopsis*. *Mol. Cell* 66: 648–657.e4.

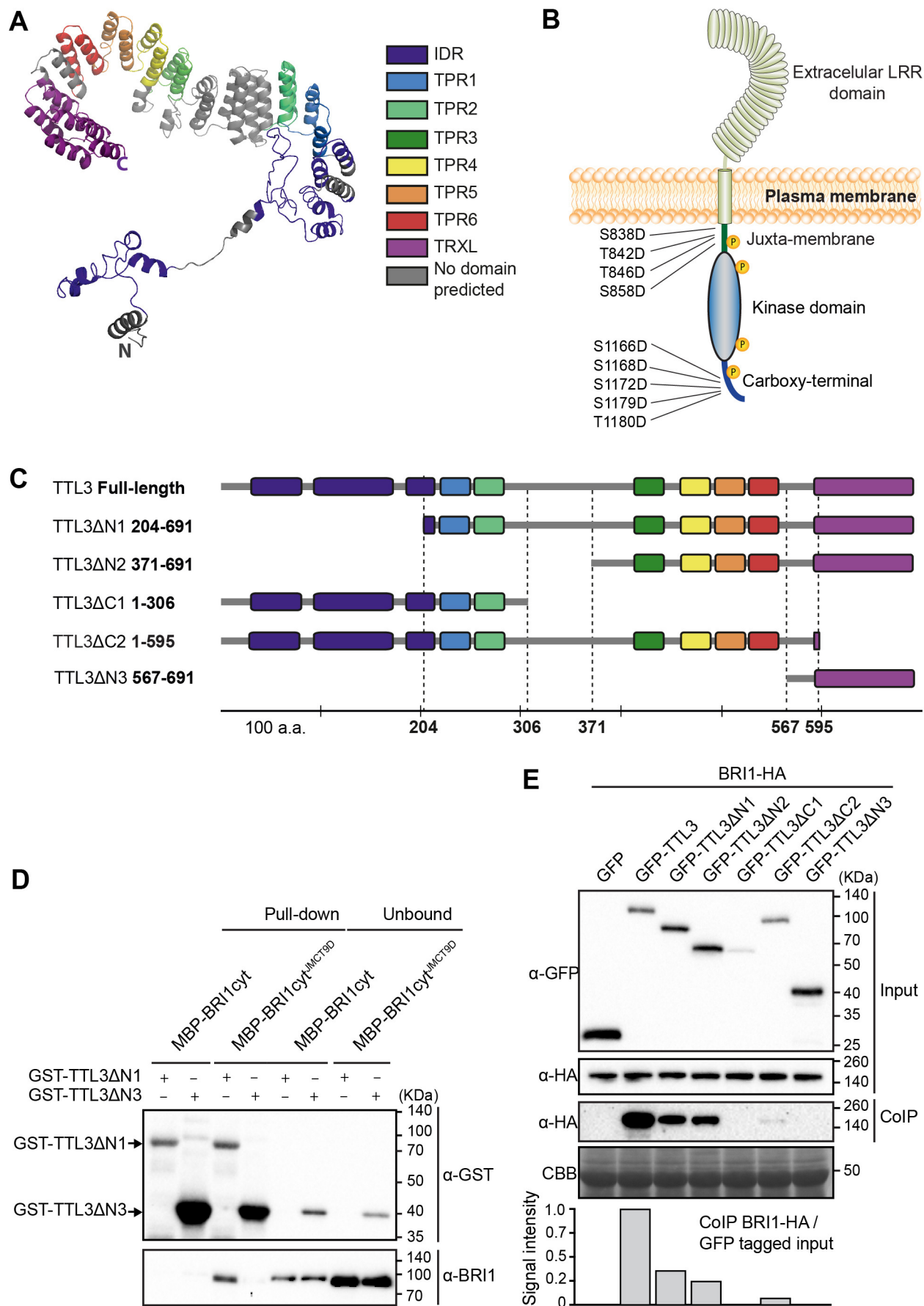


**Figure 1. TTL3 interacts with BRI1 *in vivo* and *in vitro*.**

(A) The structural model of TTL3 protein predicted *in silico* using I-TASSER server (Zhang, 2008) and processed by PyMOL (Schrödinger). IDR, intrinsically disordered region; TPR, tetratricopeptide repeats; and TPRX thioredoxin-like domain with homology to thioredoxins; N; N-terminus; C; C-terminus.

**(B)** Schematic representation of BRI1 protein and the nine Serine/Threonine residues of the juxta-membrane and carboxyl-terminal domains that were substituted by Aspartic Acid in the BAK1-independent BRI1-constitutive (phosphomimetic) active form BRI1cyt<sup>JMCT9D</sup> (Wang et al., 2008).

**(C)** Schematic representations of full-length and different truncated versions of TTL3 protein. Numbers indicate first and last amino acids of TTL3 truncated proteins. IDR, intrinsically disordered region; TPR, tetratricopeptide repeats; TPRX, thioredoxin-like domain with homology to thioredoxins; domains and protein fragments interspersing the conserved domains are represented with the same color code as in **(A)**.

**(D)** TTL3 $\Delta$ N1 interacts with BRI1cyt<sup>JMCT9D</sup> *in vitro*, as shown by a GST-pull down assay. GST-TTL3 $\Delta$ N1 and GST-TTL3 $\Delta$ N3 were detected with anti-GST antibody. MBP-BRI1cyt and MBP-BRI1cyt<sup>JMCT9D</sup> were detected using specific anti-BRI1 antibodies (Bojar et al., 2014). Pull-down reflects 20% of the total pulled-down proteins. Unbound reflects 1% of the total unbound fraction.

**(E)** BRI1-HA co-immunoprecipitates with GFP-TTL3 full length and GFP-TTL3 truncated versions  $\Delta$ N1,  $\Delta$ N2 and  $\Delta$ C1. Numbers indicate first and last amino acids of TTL3 truncated proteins. BRI1-HA was transiently co-expressed in *N. benthamiana* with GFP-TTL3 full length and truncated versions and GFP tagged protein was immunoprecipitated using anti-GFP Trap beads. Total (input), immunoprecipitated (IP) and Co-Immunoprecipitated (CoIP) proteins were analyzed by immunoblotting. Equal loading was confirmed by Coomassie blue staining (CBB) of input samples. GFP and HA tagged proteins were detected with anti-GFP and anti-HA antibody, respectively. The amount of co-immunoprecipitated BRI1-HA was normalized relative to the amount of GFP tagged protein from the input, dividing the signal intensity of co-IP BRI1-HA by the signal intensity of the each GFP tagged protein from the input that co-IP BRI1-HA.

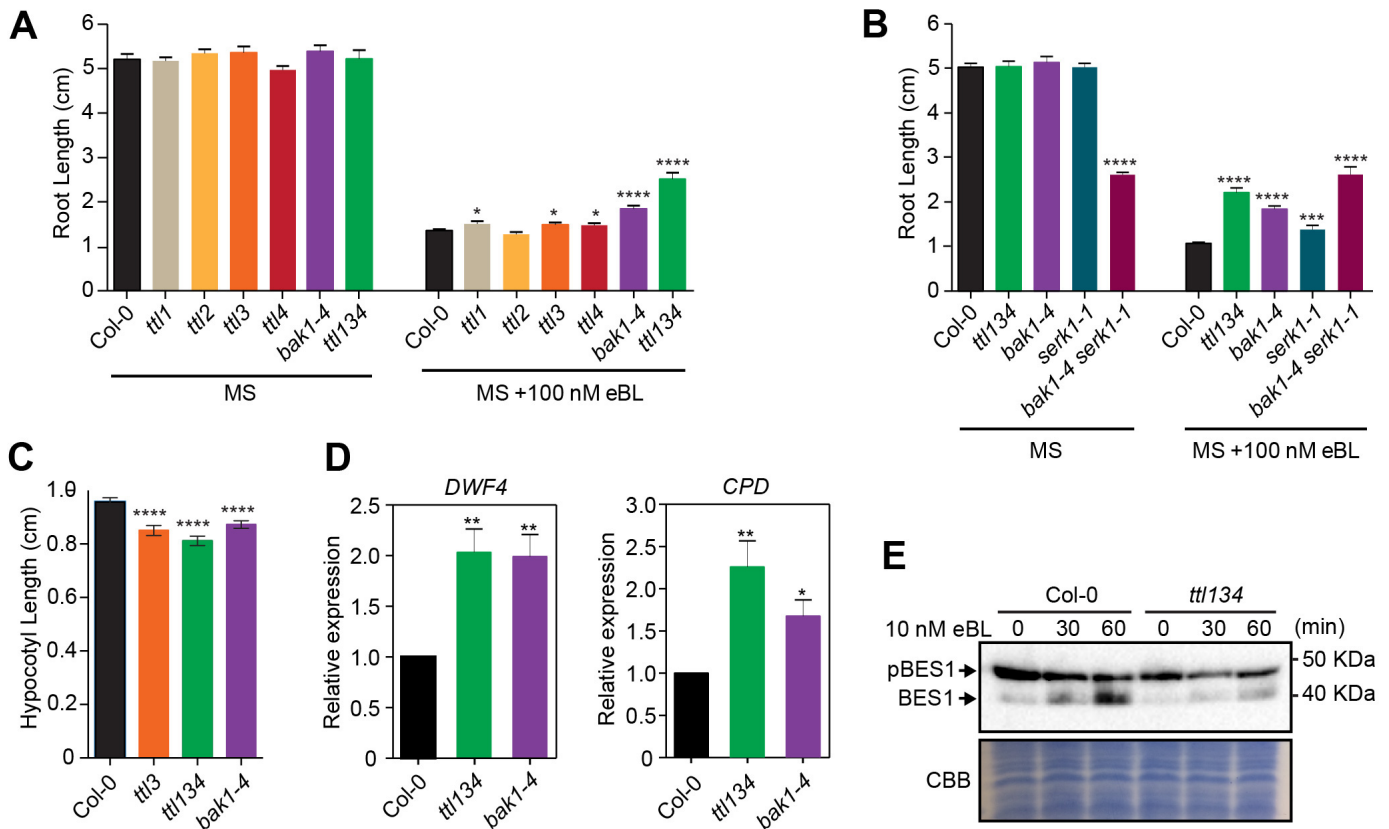


**Figure 2. *TLL1*, *TLL3* and *TLL4* genes play a positive role in BR signaling.**

**(A)** *ttl1*, *ttl3*, *ttl4* and *ttl134* show root growth hyposensitivity to BR. Statistical analysis of root length measurements of Col-0, *ttl*, and *bak1-4* mutants in control conditions (MS) and in response to epibrassinolide (eBL). Seedlings were grown in long days for 4 days in half-strength MS agar solidified medium and then transferred to half-strength MS agar solidified medium (MS) or half-strength MS agar solidified medium supplemented with 100 nM of eBL (MS + 100 nM eBL) and root length was measured 6 days later. Asterisks indicate statistical differences between mutant vs Col-0 determined by the unpaired *t*-test (\*  $P \leq 0.05$ , \*\*  $P \leq 0.01$ , \*\*\*  $P \leq 0.001$ , \*\*\*\*  $P \leq 0.0001$ ). Data represent mean values, error bars are SEM,  $n \geq 35$  seedlings per experiment. The experiment was repeated three times with similar results.

**(B)** Root length responses to eBL of wild-type Col-0, *ttl134* and BR perception mutants. Seedlings were grown and root length was analyzed as described in **(A)**. Asterisks indicate statistical differences between mutant vs Col-0 as determined by the unpaired *t*-test (\*\*\*  $P \leq 0.001$ , \*\*\*\*  $P \leq 0.0001$ ). Data represent mean values, error bars are SEM,  $n=30$  seedlings per experiment. The experiment was repeated three times with similar results.

**(C)** Defective hypocotyl elongation in *ttl* mutants. Col-0, *ttl3*, *ttl134* and *bak1-4* seedlings were grown for 4 days in long-day photoperiod in half-strength MS agar solidified medium. Seedlings with the same size were then placed in the dark and hypocotyl elongation was measured 3 days later. Asterisks indicate statistically significant differences between Col-0 and the indicated genotype as determined by the unpaired *t*-test (\*\*\*\*  $P \leq 0.0001$ ), values are mean, error bars are SEM,  $n = 80$  seedlings per experiment. The experiment was repeated twice with similar results.

**(D)** BR-responsive genes *DWF4* and *CPD* show induced expression in *ttl134* and *bak1-4* relative to Col-0 seedlings. Seeds were germinated in half-strength MS agar solidified medium and grown vertically in long-day photoperiod conditions. 5-day-old seedlings were transferred to half-strength MS liquid medium and after 5 days of acclimation, the relative expression level of *DWF4* and *CPD* was measured by quantitative reverse transcriptase PCR (qPCR). The expression of *DWF4* and *CPD* was first normalized to the expression of *ACTIN2* and represented relative to the expression of Col-0. The data are shown as mean  $\pm$  SEM from at least three independent biological replicates (pool of 20 seedlings per biological replicate). Asterisks indicate statistically significant differences between the indicated genotype vs Col-0 as

determined by the unpaired t-test (\*  $P \leq 0.05$ , \*\*  $P \leq 0.01$ ). The experiment was repeated three times with similar results.

**(E)** Phosphorylation status of BES1 in response to exogenously applied BR in *Arabidopsis Col-0* and *tt134*. Ten-day-old seedlings pre-treated for 3 days with the BR biosynthetic inhibitor brassinazole (BRZ) to deplete the endogenous pool of BRs were subjected to 10 nM eBL treatment for 0, 30 and 60 minutes. Total proteins from a pool of 20 seedlings were analyzed by an immunoblot assay with a specific anti-BES1 antibody (Yu et al., 2011). The upper band corresponds to phosphorylated BES1 (pBES1) and the lower one to dephosphorylated BES1 (BES1). The experiment was repeated two times with similar results.

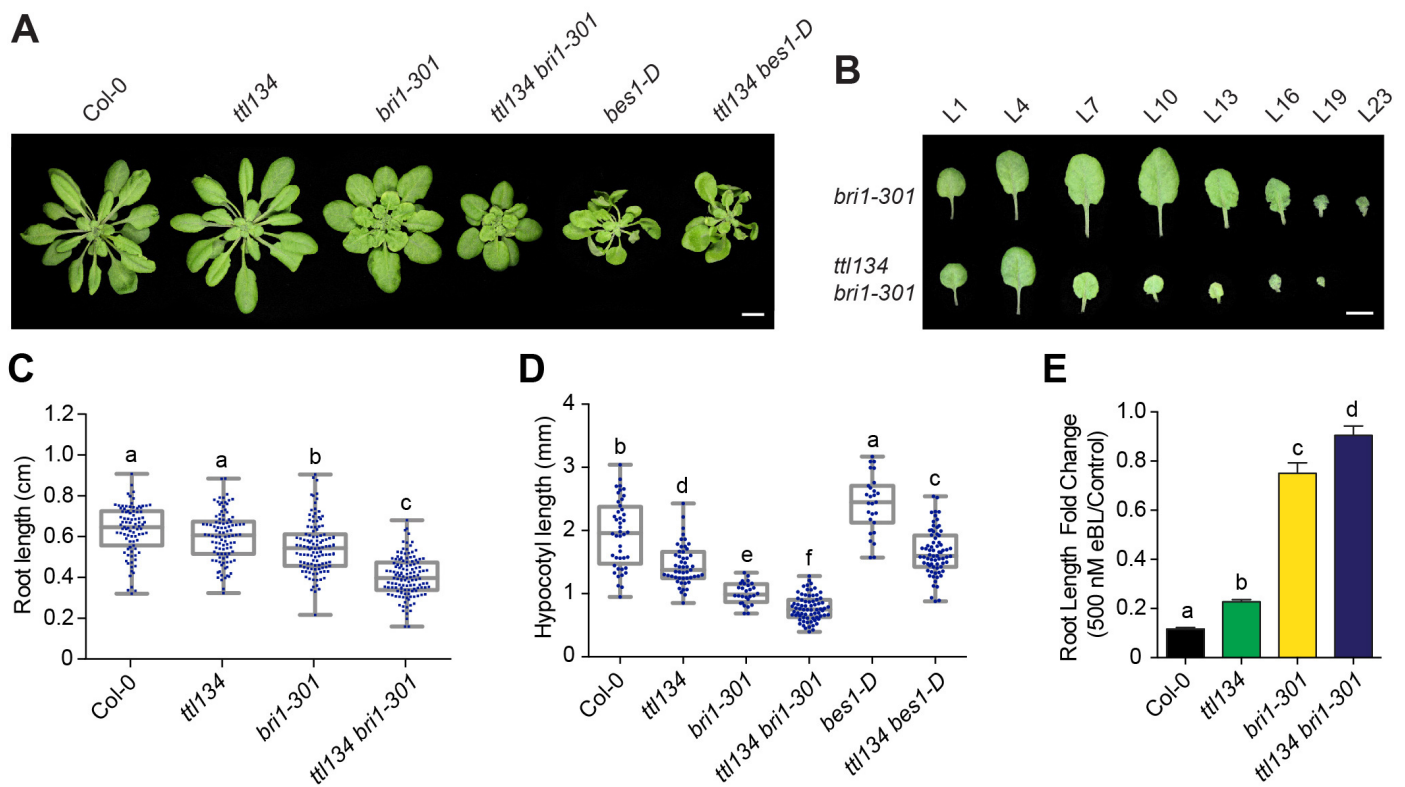


**Figure 3. *tt134* mutations enhance the *bri1-301* defective phenotype and partially reduce the BR responses in *bes1-D*.**

**(A)** Morphological phenotypes of 5-week-old plants grown in short-days. Scale bar represents 1 cm.

**(B)** Detached leaves of 5-week-old plants grown in short-days (L1, oldest leaf; L23 youngest leaf). Scale bar represents 1 cm.

**(C)** Root length of 3-day-old seedlings grown in long-days in half-strength MS-agar solidified medium. Dots represent individual measurements from three independent experiments. n denotes measurement of roots from independent seedlings: Col-0 (n = 92), *tt134* (n = 100), *bri1-301* (n = 113) and *tt134 bri1-301* (n = 123). Box plots display the first and third quartiles, split by the median; whiskers extend to include the maximum and minimum values. Different lowercase letters indicate significant differences. Data was analyzed with one-way ANOVA and Tukey's multiple comparison test; P < 0.05.

**(D)** Hypocotyl length of 7-day-old seedlings grown in long-days in half-strength MS-agar solidified medium. Dots represent individual measurements from three independent experiments. n denotes measurement of hypocotyls from independent seedlings: Col-0 (n = 44), *tt134* (n = 51), *bri1-301* (n = 28), *tt134 bri1-301* (n = 73), *bes1-D* (n = 27) and *tt134 bes1-D* (n = 71). Values are plotted and statistically analyzed as in **(C)**.

**(E)** Root length fold changes of seedlings grown for 7 days in the absence (Control) or presence of 500 nM of eBL in long-days. Values are mean, error bars are SEM, and n = 22 seedlings per experiment. Different lowercase letters indicate significant differences. Data were analyzed with one-way ANOVA and Tukey's multiple comparison test; P < 0.05. The experiment was repeated twice with similar results.

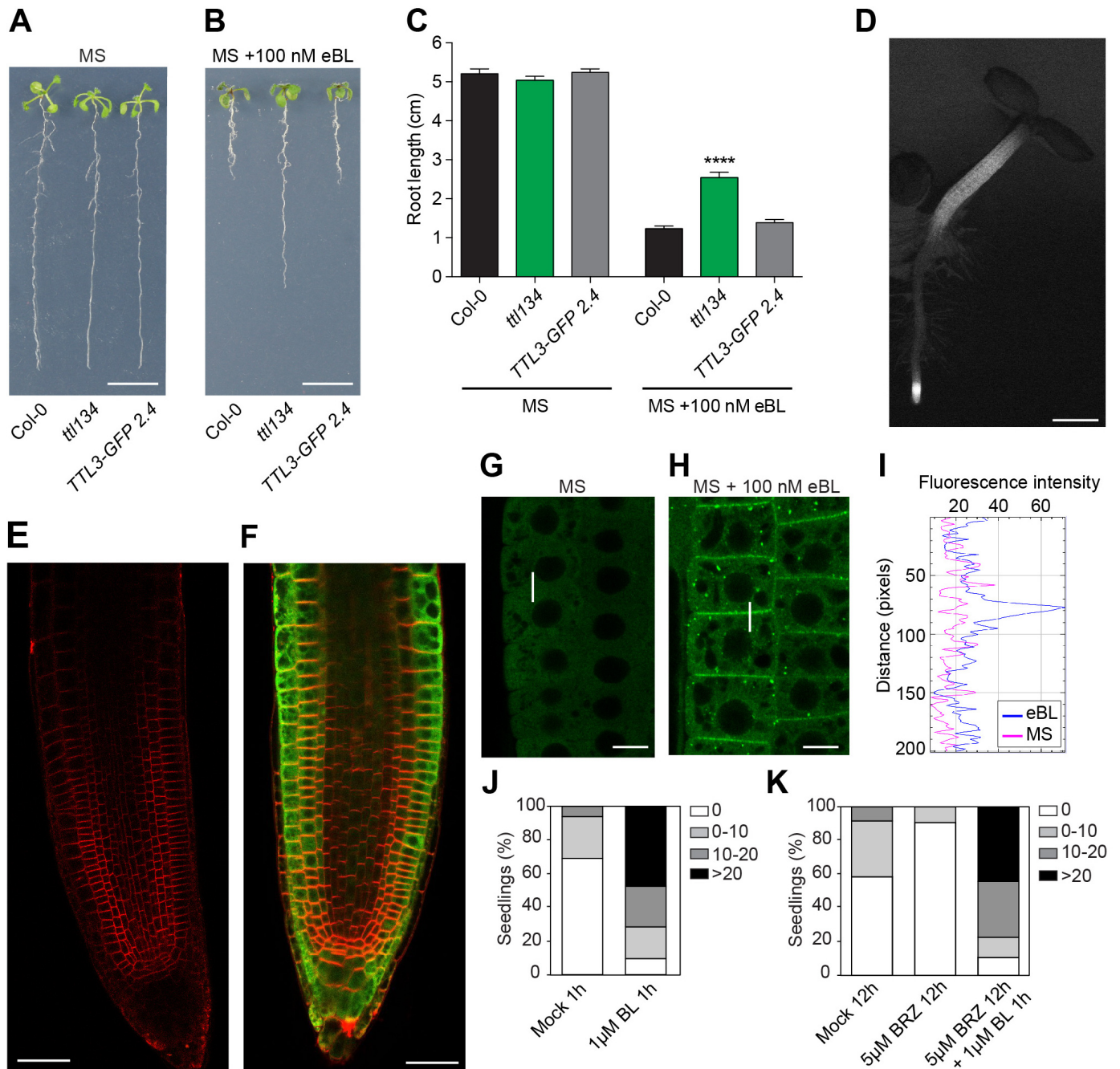


**Figure 4. BRs regulate the cytoplasmic/plasma membrane localization of TTL3**

(A, B and C) The root growth responses to eBL of the *ttl134* triple mutant are complemented in *TTL3-GFP 2.4*. Seedlings were grown for 4 days in half-strength MS agar solidified medium and then transferred to half-strength MS agar solidified medium (A) or half-strength MS agar solidified medium supplemented with 100 nM of Brassinolide (B). (A and B) Representative photographs of seedlings, 6 days after being transferred to control or eBL treatment. Scale bar represents 1 cm. (C) Statistical analysis of root length of Col-0, *ttl134* and the complementation line *TTL3-GFP 2.4*. Asterisks indicate statistically significant differences between the indicated genotype vs Col-0 as determined by the unpaired *t*-test (\*\*\*\*  $P \leq 0.0001$ ). Data represent mean values, error bars are SEM, and  $n=30$  seedlings per experiment. The experiment was repeated three times with similar results.

(D) Expression pattern of *TTL3-GFP* in 3-day-old *TTL3-GFP 2.4* Arabidopsis seedlings. Images were captured using conventional wide field fluorescence microscopy with a GFP filter. Scale bar represents 500  $\mu$ m.

(E and F) Longitudinal median section of root tips of a 3-day-old Col-0 (E) and *TTL3-GFP 2.4* seedling as observed by laser scanning confocal microscopy (F). Images are a merge of green channel showing TTL3-

GFP expression and red channel showing plasma membrane stained with FM4-64. Scale bar represents 20  $\mu\text{m}$ .

**(G, H and I)** Confocal images showing localization of TTL3-GFP in epidermal cells from the root meristematic zone in 4-day-old *Arabidopsis TTL3-GFP 2.4* in half-strength MS agar solidified medium, in control conditions (1 hour treatment with eBL solvent) **(G)** or after 1 hour of 1  $\mu\text{M}$  eBL treatment **(H)** in half-strength MS agar liquid medium. Scale bar represents 10  $\mu\text{m}$  (horizontal bar). **(I)** Quantification of fluorescent protein signal in plasma membrane vs cytoplasm. Line scan measurements spanning membrane and cytoplasm were carried out (represented in **(G)** and **(H)** as a vertical white line), and representative plot profiles of sample measurements are presented.

**(J and K)** Quantification of the cytoplasmic and PM localization of TTL3-GFP in 4-day-old *Arabidopsis TTL3-GFP 2.4* seedlings treated for 1 hour with 1  $\mu\text{M}$  eBL **(J)** or pre-treated for 12 hours with 5  $\mu\text{M}$  BRZ prior to 1  $\mu\text{M}$  eBL application for 1 hour **(K)**. The number of cells with dual cytoplasmic/plasma membrane localization in meristematic and transition zone was counted for each analyzed root using confocal microscopy. Seedlings were grouped in categories according to the number of cells that presented this dual localization, and the percentage of seedlings displaying each category depicted in the key was calculated. Represented categories in the key indicate the number of cells per seedling with dual cytoplasmic/plasma membrane localization. At least 16 seedlings per treatment, and approximately 200 cells (cell from epidermis, cortex and endodermis all combined) per seedling of the meristematic region of the root tip were analyzed.

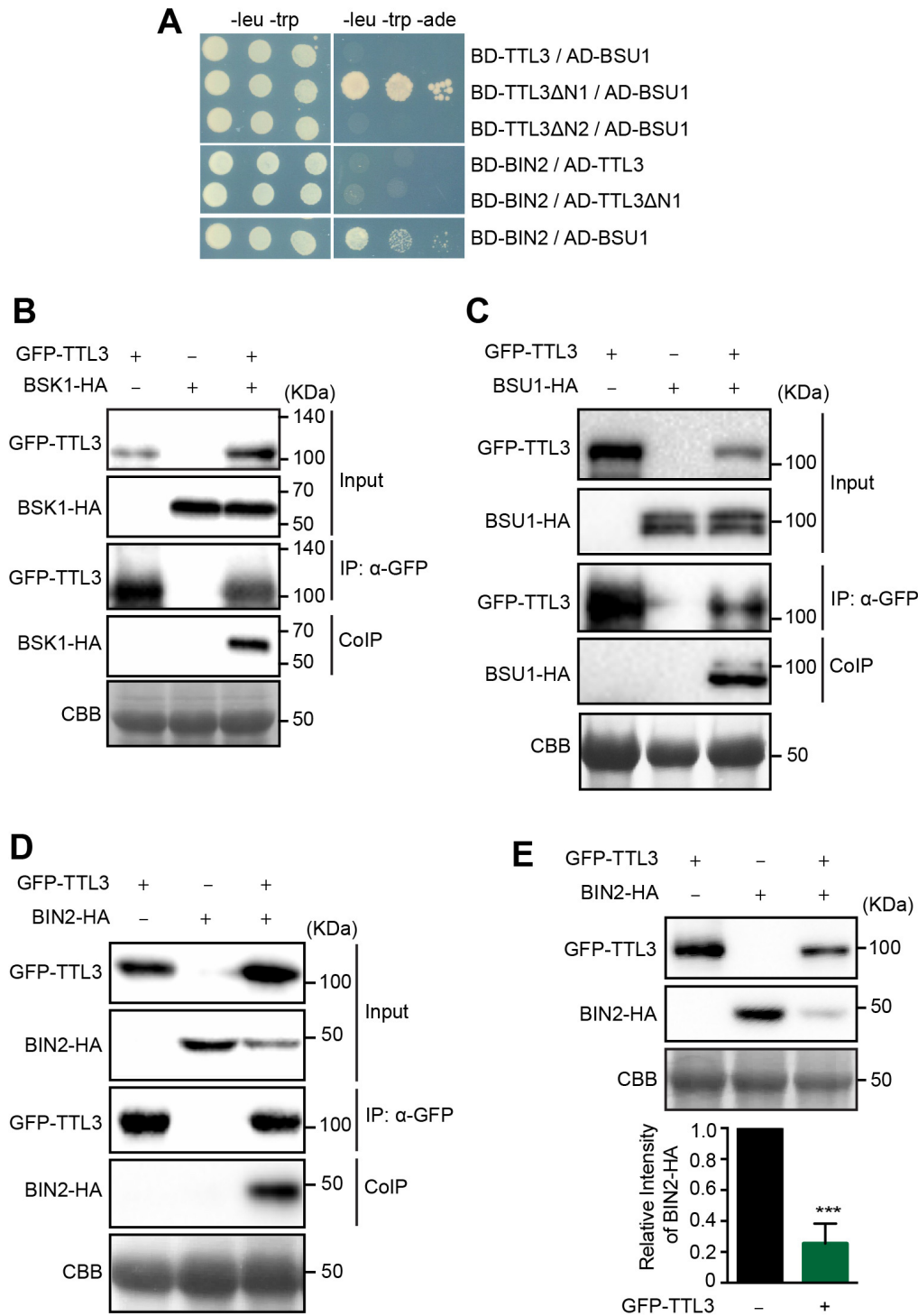


**Figure 5. TTL3 associates with BSK1 and BIN2 and directly interacts with BSU1.**

**(A)** Yeast-two-hybrid assays to determine the interaction of full-length TTL3, the TTL3 fragment TTL3ΔN1 (amino acid 204–691) and the TTL3 fragment TTL3ΔN2 (amino acid 371–691) with BIN2 and BSU1. Growth on plasmid-selective media (left column) and interaction-selective media (lacking adenine, right column) are shown.

**(B)** BSK1 co-immunoprecipitates with TTL3. BSK1-HA and GFP-TTL3 were transiently expressed in *N. benthamiana*. GFP-TTL3 was immunoprecipitated with anti-GFP Trap beads. Total (input), immunoprecipitated (IP) and Co-Immunoprecipitated (CoIP) proteins were analyzed by immunoblotting. Equal loading was confirmed by Coomassie blue staining (CBB) of input samples. GFP-TTL3 and BSK1-HA were detected with anti-GFP and anti-HA antibody, respectively.

**(C)** BSU1 co-immunoprecipitates with TTL3. GFP-TTL3 and BSU-HA proteins were transiently expressed in *N. benthamiana*, immunoprecipitated and analyzed as described in **(B)**. GFP-TTL3 and BSU1-HA were detected with anti-GFP and anti-HA antibodies, respectively.

**(D)** BIN2 co-immunoprecipitates with TTL3. BIN2-HA and GFP-TTL3 proteins were expressed in *N. benthamiana*, immunoprecipitated, and analyzed as described in **(B)**. GFP-TTL3 and BSU1-HA were detected with anti-GFP and anti-HA, respectively.

**(E)** TTL3 promotes BIN2 depletion. BIN2-HA with and without GFP-TTL3 was expressed in *N. benthamiana*. Protein extracts were analyzed by immunoblotting. Equal loading was confirmed by Coomassie blue staining (CBB) of input samples. GFP-TTL3 and BIN2-HA were detected with anti-GFP and anti-HA antibody, respectively. Bottom panel represents the signal density of BIN2-HA co-expressed with or without GFP-TTL3 in *N. benthamiana* was quantified based on the six biological repeats. The immunoblot signal intensity of BIN2-HA co-expressed with GFP-TTL3 was normalized to the immunoblot signal intensity of BIN2-HA co-expressed with a empty vector. Asterisks indicate statistical differences as determined by the unpaired *t*-test (\*\**P* ≤ 0.001).

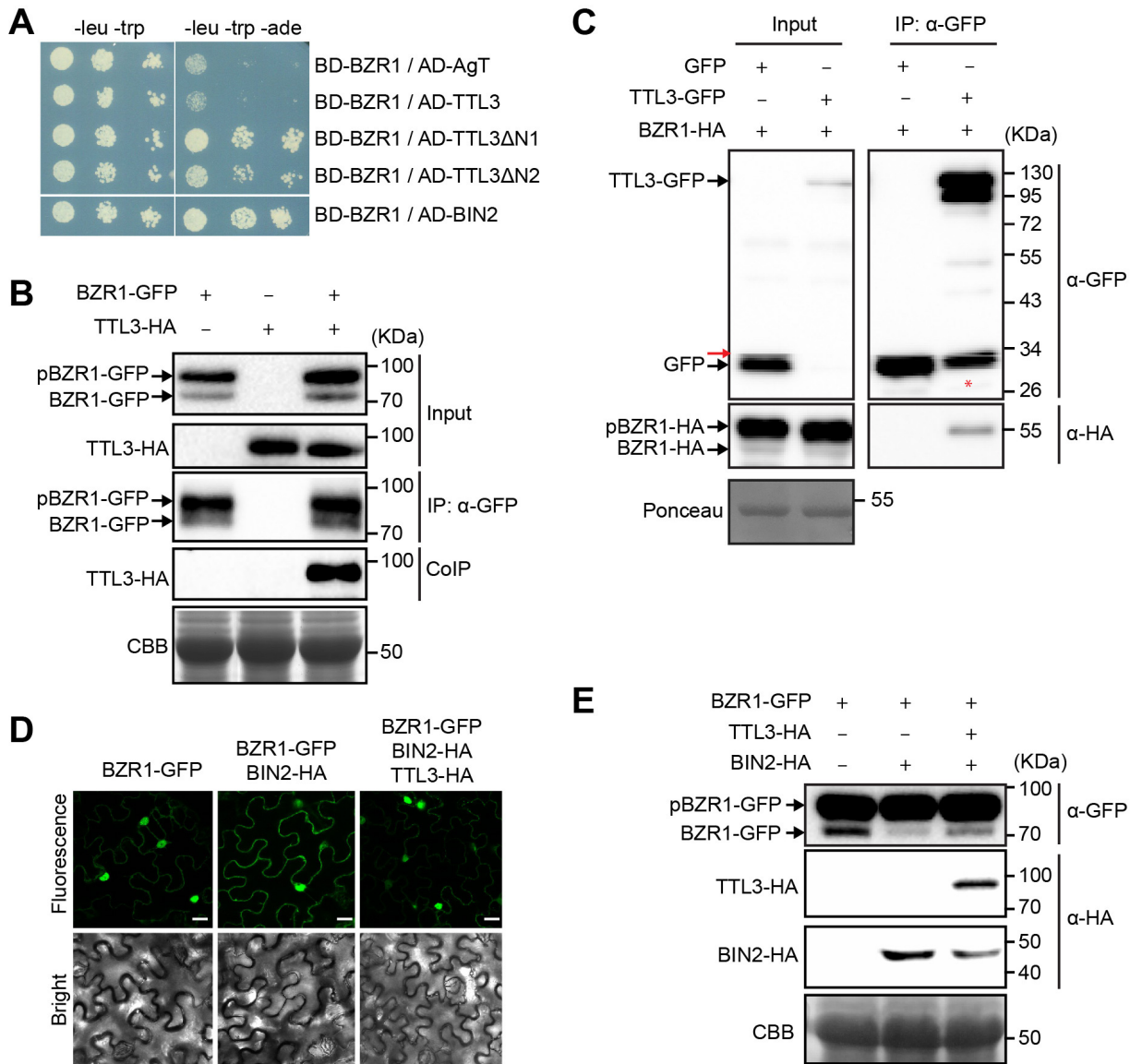


**Figure 6. TTL3 interacts with BZR1 and regulates its cytoplasmic/nuclear localization.**

**(A)** Yeast-two-hybrid assays to determine the interaction of BZR1 with TTL3, the TTL3 fragment TTL3ΔN1 (amino acid 204–691), the TTL3 fragment TTL3ΔN2 (amino acid 371–691) and BIN2. Interaction of BZR1 with a fragment of SV40 large T-antigen (AD-AgT) was also included to show BD-BZR1 self-activation capacity. Growth on plasmid-selective media (left column) and interaction-selective media (lacking adenine, right column) are shown.

**(B)** TTL3 co-immunoprecipitates with BZR1. TTL3-HA and BZR1-GFP were transiently expressed in *N. benthamiana*. BZR1-GFP was immunoprecipitated with anti-GFP Trap beads. Total (input), immunoprecipitated (IP) and Co-Immunoprecipitated (CoIP) proteins were analyzed by immunoblotting. Equal loading was confirmed by Coomassie blue staining (CBB) of input samples. BZR1-GFP and TTL3-HA were detected with anti-GFP and anti-HA, respectively. The upper band corresponds to phosphorylated BZR1 (pBZR1-GFP) and the lower one to dephosphorylated BZR1 (BZR1-GFP).

**(C)** Co-immunoprecipitation of BZR1-HA with TTL3-GFP expressed in transfected Arabidopsis Col-0 protoplasts. Samples were analyzed as in **(B)**. Protoplasts co-transfected with free GFP and BZR1-HA, were used as a negative control for Co-IP. Equal loading was confirmed by Ponceau staining of input samples. TTL3-GFP and free GFP were detected with anti-GFP antibody and BZR1-HA was detected with anti-HA antibody. Asterisk indicates GFP that results from proteolytic cleavage of TTL3-GFP. Red arrow indicates an artefact from imaging the blot with high sensitivity using an Azure c300 Chemiluminescent Western Blot Imaging System.

**(D)** TTL3 abolishes the cytoplasmic retention of BZR1 by BIN2. Subcellular localization of BZR1-GFP alone, co-expressed with BIN2-HA, and with BIN2-HA and TTL3-HA in *N. benthamiana* leaves. Images of the GFP signal were obtained using laser scanning confocal microscopy. Images show a single equatorial plane in *N. benthamiana* leaves. Scale bars represent 20  $\mu\text{m}$ . The experiment was repeated three times with similar results.

**(E)** Immunoblot analysis of the BZR1-GFP proteins transiently expressed alone, co-expressed with BIN2-HA, and co-expressed with BIN2-HA and TTL3-HA in *N. benthamiana* leaves observed by confocal microscopy in **(D)**. Proteins were analyzed by immunoblotting. Equal loading was confirmed by Coomassie blue staining (CBB) of input samples. BZR1-GFP was detected with anti-GFP antibody, while TTL3-HA and BIN2-HA were detected with anti-HA antibody. In the anti-GFP blot, the upper band corresponds to phosphorylated BZR1 (pBZR1-GFP) and the lower one to dephosphorylated BZR1 (BZR1-GFP).

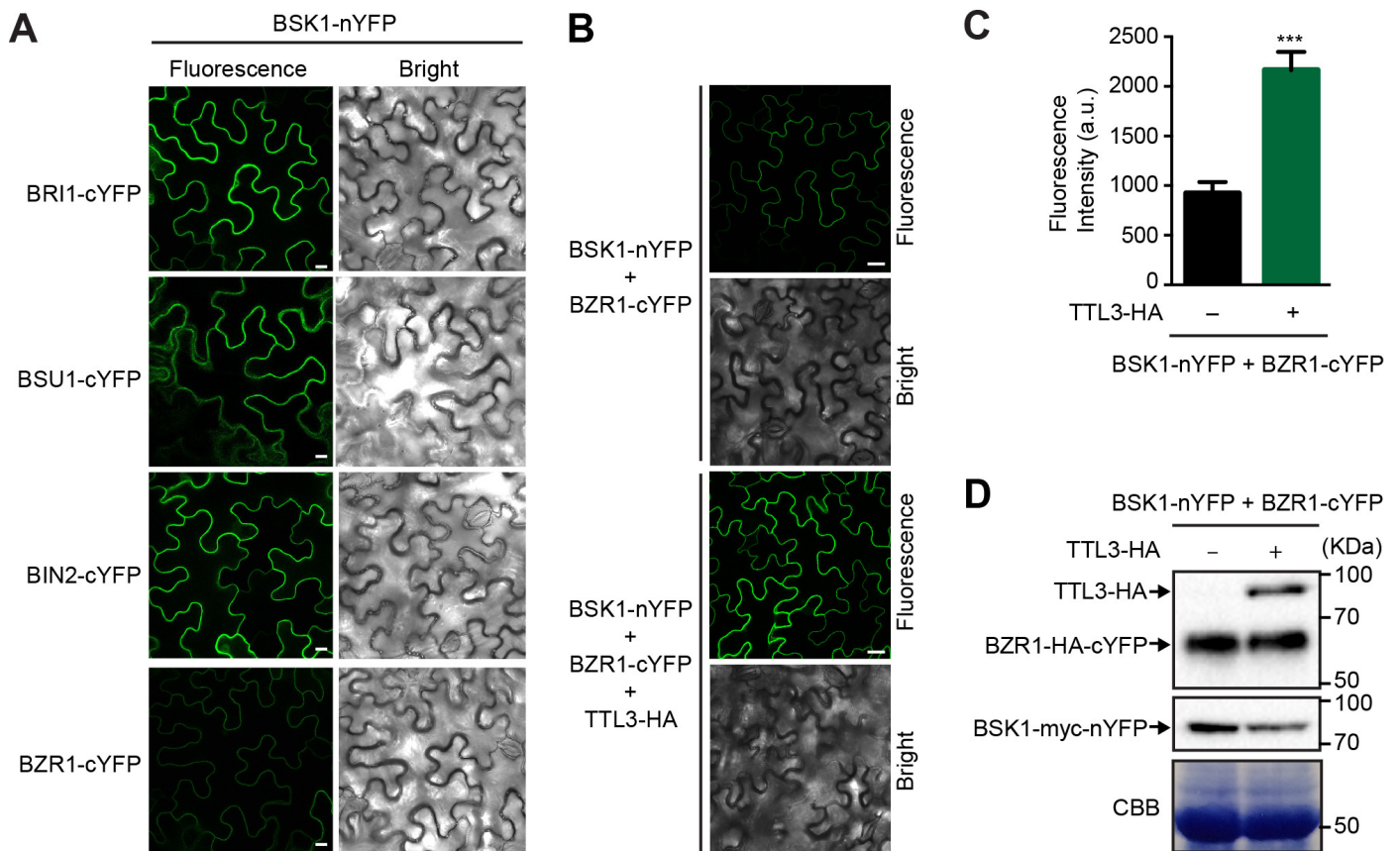


**Figure 7. Co-expression of TTL3 enhances pBZR1-BSK1 interaction.**

**(A)** BiFC shows strong association of BSK1 with BRI1, BSU1, and BIN2 and weak association with BZR1. *N. benthamiana* leaves were co-agroinfiltrated with the *Agrobacterium* strains harboring a construct to express the BSK1 protein fused to the N-terminus half of YFP and the BRI1, BSU1, BIN2 or BZR1 proteins fused to the C-terminus half of YFP and observed under a laser scanning confocal microscope. Strong fluorescence signals are observed when BSK1-nYFP is co-expressed with BRI1-cYFP, BSU1-cYFP or BIN2-cYFP. A faint YFP signal is observed when BSK1-nYFP is co-expressed with BZR1-cYFP. From left to right columns, images show BiFC YFP fluorescence in green and bright field. Scale bars represent 20  $\mu$ m. The experiment was repeated two times with similar results.

**(B)** Expression of TTL3 increases the weak BiFC association of BSK1 and BZR1. *N. benthamiana* leaves were co-agroinfiltrated with the *Agrobacterium* strains harboring the corresponding constructs to express the BSK1 protein fused to the N-terminus half of YFP and the BZR1 protein fused to the C-terminus half of YFP. *N. benthamiana* leaves were pre-treated with 5  $\mu$ M eBL for 3 hours before confocal imaging analysis. Co-expression of TTL3-HA together with BSK1-nYFP and BZR1-cYFP highly enhances the GFP signal. From left to right columns, BiFC YFP fluorescence in green and bright field. Scale bars represent 20  $\mu$ m. The experiment was repeated three times with similar results.

**(C)** Quantification of the BiFC fluorescence intensity of BSK1 and BZR1 in the presence or absence of TTL3-HA described in **(B)**. Asterisks indicate statistical differences between BiFC fluorescence intensity of BSK1 and BZR1 in the absence or presence of TTL3-HA determined by the unpaired t-test (\*\*\*)  $P \leq 0.001$ . Data represent mean values, error bars are SEM, and  $n=5$  randomly chosen regions of infiltrated leaves. The experiment was repeated three times with similar results. Arbitrary units (a.u.).

**(D)** Immunoblot analysis reveals similar amounts of BSK1-nYFP and BZR1-cYFP when co-expressed with or without TTL3-HA. Proteins were transiently expressed as described in **(B)**. Equal loading was confirmed by Coomassie blue staining (CBB) of total proteins. BSK1-nYFP contains a myc tag (BSK1-myc-nYFP) and was detected using anti-myc antibody, while BZR1-cYFP contains a HA tag (BZR1-HA-cYFP) and was detected using an anti-HA antibody. TTL3-HA was also detected with an anti-HA antibody. The experiment was repeated three times with similar results.